

AWARD NUMBER: W81XWH-13-2-0087

TITLE: Optimization of Soft Tissue Management, Spacer Design, and Grafting Strategies for Large Segmental Bone Defects using the Chronic Caprine Tibial Defect Model

PRINCIPAL INVESTIGATORS: Dr. Pluhar

CONTRACTING ORGANIZATION:
Regents of the University of Minnesota
Minneapolis, MN 55455

REPORT DATE: **December 2016**

TYPE OF REPORT: **Final**

PREPARED FOR: U.S. Army Medical Research and Materiel Command
Fort Detrick, Maryland 21702-5012

DISTRIBUTION STATEMENT: Approved for Public Release;
Distribution Unlimited

The views, opinions and/or findings contained in this report are those of the author(s) and should not be construed as an official Department of the Army position, policy or decision unless so designated by other documentation.

REPORT DOCUMENTATION PAGE			<i>Form Approved</i> <i>OMB No. 0704-0188</i>		
<small>Public reporting burden for this collection of information is estimated to average 1 hour per response, including the time for reviewing instructions, searching existing data sources, gathering and maintaining the data needed, and completing and reviewing this collection of information. Send comments regarding this burden estimate or any other aspect of this collection of information, including suggestions for reducing this burden to Department of Defense, Washington Headquarters Services, Directorate for Information Operations and Reports (0704-0188), 1215 Jefferson Davis Highway, Suite 1204, Arlington, VA 22202-4302. Respondents should be aware that notwithstanding any other provision of law, no person shall be subject to any penalty for failing to comply with a collection of information if it does not display a currently valid OMB control number. PLEASE DO NOT RETURN YOUR FORM TO THE ABOVE ADDRESS.</small>					
1. REPORT DATE December-2016		2. REPORT TYPE Final Report		3. DATES COVERED 30 Sep 2013 - 29 Sep 2016	
4. TITLE AND SUBTITLE Optimization of Soft Tissue Management, Spacer Design, and Grafting Strategies for Large Segmental Bone Defects using the Chronic Caprine Tibial Defect Model			5a. CONTRACT NUMBER		
			5b. GRANT NUMBER W81XWH-13-2-0087		
			5c. PROGRAM ELEMENT NUMBER		
6. AUTHOR(S) Dr. G. Elizabeth Pluhar E-Mail(s): pluha006@umn.edu			5d. PROJECT NUMBER		
			5e. TASK NUMBER		
			5f. WORK UNIT NUMBER		
7. PERFORMING ORGANIZATION NAME(S) AND ADDRESS(ES) <div style="text-align: right;">Regents of the University of Minnesota 200 Oak Street SE Minneapolis, MN. 55455-2009</div>			8. PERFORMING ORGANIZATION REPORT		
9. SPONSORING / MONITORING AGENCY NAME(S) AND ADDRESS(ES) U.S. Army Medical Research and Materiel Command Fort Detrick, Maryland 21702-5012			10. SPONSOR/MONITOR'S ACRONYM(S)		
			11. SPONSOR/MONITOR'S NUMBER(S)		
12. DISTRIBUTION / AVAILABILITY STATEMENT Approved for Public Release; Distribution Unlimited					
13. SUPPLEMENTARY NOTES					
14. ABSTRACT This proposal addresses the treatment of segmental bone defects and methods that can be used to manipulate the Masquelet induced membrane to create a graft bed that optimizes bone regeneration. The effect of surgical management of the IM demonstrated a significant benefit of scraping to remove the inner layer of the IM (p=0.041). In contrast, modifying the texture on the PMMA spacer to double the surface area of the IM did not result in improved bone regeneration. This finding can be immediately translated into clinical practice. This study highlights the fact that the Chronic Caprine Tibial Defect Model is sufficiently sensitive to detect variations and represents a suitable clinically relevant animal model for testing new therapies for bone regeneration.					
15. SUBJECT TERMS Optimization of the Masquelet induced membrane to improve bone healing.					
16. SECURITY CLASSIFICATION OF:			17. LIMITATION OF ABSTRACT	18. NUMBER OF PAGES	19a. NAME OF RESPONSIBLE PERSON USAMRMC
a. REPORT U	b. ABSTRACT U	c. THIS PAGE U			19b. TELEPHONE NUMBER (include area code)

Table of Contents

	<u>Page</u>
1. Introduction.....	4
2. Keywords.....	4
3. Overall Project Summary.....	4
4. Key Research Accomplishments.....	31
5. Conclusion.....	32
6. Publications, Abstracts, and Presentations.....	33
7. Inventions, Patents and Licenses.....	33
8. Reportable Outcomes.....	33
9. Other Achievements.....	34
10. References.....	34
11. Appendices.....	35

1. INTRODUCTION:

High-energy extremity fractures with soft tissue involvement affect thousands of U.S. Service members each year [1]. These injuries are complex in nature, typically involving large regions of bone damage or loss and are often associated with loss of other tissues such as skin, bone, muscle, cartilage, blood vessels, and nerves. In some cases, these injuries also are complicated by infection. Despite substantial advances in the availability and variety of bone graft substitute materials in recent years, these large bone defects remained a clinical challenge. Additionally, although a massive amount of research on bone defects has been done with astoundingly good results in animal models, human clinical results are mediocre at best. This research specifically addresses the treatment of segmental bone defects with methods that optimize the Masquelet induced membrane [2-6] to create a superior graft bed for bone regeneration. Using the Chronic Caprine Tibial Defect (CCTD) model, this study specifically aims to assess the effects of surgical technique and spacer design to optimize the biology of the induced membrane (IM), and to define the characteristics of an optimal membrane with respect to the parameters of cell composition, histology, and gene expression. Optimizing the Masquelet IM method and characterizing the biological features of the IM has significant potential to enhance the clinical care of wounded warriors who require bone regeneration procedures and to guide the ongoing development of advanced methods for bone regeneration. This program includes a nested development program for Dr. Jean-Claude D'Alleyrand, a junior orthopaedic surgeon at the Walter Reed National Military Medical Center, to nurture his interest in translational and clinical research by fostering relationships with established, independent clinician scientists with proven track records.

The Specific Aims of this proposal were as follows:

Aim 1 – Test the hypothesis that removal of the thin inner surface of the IM created around a smooth polymethylmethacrylate (PMMA) spacer will enhance bone regeneration.

Aim 2 - Test the hypothesis that the IM created by a textured PMMA spacer will enhance bone regeneration compared to that of a smooth PMMA spacer.

Aim 3 – Characterize the histological, biochemical, cellular and gene expression features of the IM and define the features that best predict the magnitude of bone regeneration with autogenous cancellous bone graft (ACBG).

The broad objective of our team is to accelerate the rate at which clinically significant questions related to surgical management of the induced membrane, advanced spacer design, and advanced bone regeneration strategies can be translated into clinical practice to improve the care of wounded warriors and civilians.

2. KEYWORDS: segmental bone defect, caprine, tibia, animal model, chronic, bone graft, Masquelet technique, induced membrane, bone regeneration, surgical technique, spacer

3. OVERALL PROJECT SUMMARY:

3.1 Overall Summary for Aim 1 and Aim 2:

***Aim 1:** Test the hypothesis that removal of the thin inner surface of the IM created around a smooth polymethylmethacrylate (PMMA) spacer will enhance bone regeneration.*

***Aim 2:** Test the hypothesis that the IM created by a textured PMMA spacer will enhance bone regeneration compared to that of a smooth PMMA spacer.*

Protocol

Thirty-two skeletally mature female goats, age 5 ± 1 years (mean \pm SD) weighing 50 ± 4 kg underwent the CCTD procedure and were randomly assigned to four groups (8 animals/group) using a 2 x 2 test matrix (factorial design). These groups included: (1) smooth spacer and intact IM; (2) smooth spacer and scraped IM; (3) textured spacer and intact IM; and (4) textured spacer and scraped IM. Study animals were cared for in accordance with the principles of the Guide for the Care and Use of Laboratory Animals after approval from the Cleveland Clinic Institutional Animal Care and Use Committee (IACUC # 2013-1021) and the Animal Care and Use Review Office of US Army Medical Research and Materiel Command (OR # 120082).

The textured spacer had a surface area that doubled the surface area of a smooth spacer.

Aim 1 (16 goats):

Group 1 – Smooth spacer and not scraped IM

Group 2 – Smooth spacer and scraped IM

Aim 2 (16 goats):

Group 1 – Textured spacer and not scraped IM

Group 2 – Textured spacer and scraped IM

Membrane		Spacer
Not Scraped	Scraped	
Smooth	8	8
Textured	8	8

Figure 1 – Test matrix used

Surgical Protocol

Each animal undergoes two surgeries defined here as: 1) the pre-procedure to create the tibia defect and the IM and 2) the treatment (4 weeks after pre-procedure). Autogenous cancellous bone graft (ACBG) is placed into the IM that is scraped in half of the goats and not scraped in the other half.

The Pre-Procedure (Figure 2A, D) is comprised of the following essential features:

1. Make a medial skin incision and excise a 5-cm segment of tibial diaphysis and periosteum.
2. Excise an additional 2 cm of periosteum on the proximal and distal bone segments.
3. Debride 10 grams of tibialis anterior and gastrocnemius muscles.
4. Place an interlocking intramedullary nail using a custom spacer to maintain 5-cm defect length.
5. Place a pre-molded 5 cm long x 2 cm diameter PMMA spacer around the nail in the defect.
6. Irrigate the wound with normal (0.9 %) saline and close the wound.

The Treatment (Figure 2B, C, E, F) is performed 4 weeks after the Pre-Procedure and is comprised of the following steps:

1. Collect 12 cc of ACBG from sternebra 4 or 5, approaching other sternebra only as needed.
2. Open the previous skin incision on the medial aspect of the tibia.
3. Open the IM surrounding the PMMA spacer using a “bomb bay door opening”.
4. Remove the spacer without damaging the membrane or nail.
5. Collect appropriate IM samples as defined below (see section b).
6. In Aim 1, the inner layer of the IM was scraped away in one half of the goats before grafting and the graft was placed in the intact IM in the remaining goats.
7. Close the IM with 3-0 nylon to provide an intrinsic marker and close the remaining tissues.

The procedures after treatment include:

- Orthogonal radiographs (anterior-posterior (AP) and mediolateral (ML) projections) of tibias every 4 weeks
- Physical examination including lameness grading daily, then biweekly starting 2 weeks after Treatment surgery.

Euthanasia is performed 12 weeks after Treatment surgery at which time tibias are harvested and fixed in 10% formalin. Micro CT and histologic analyses of regenerate tissue are then performed.

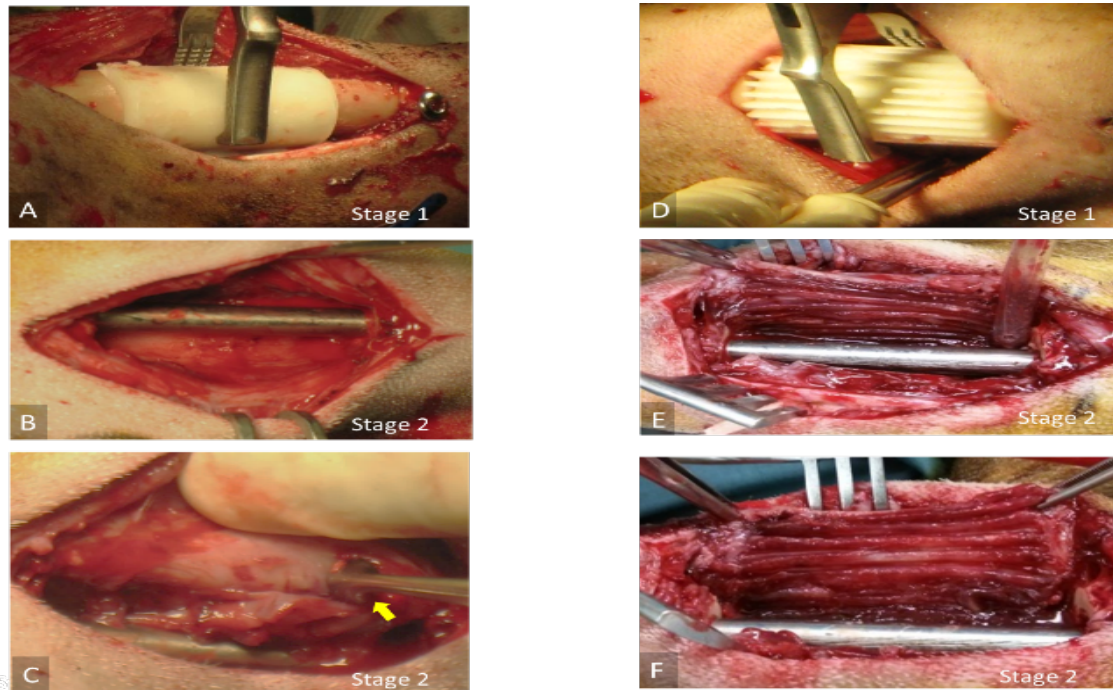


Figure 2 – Surgery pictures showing placement of a smooth spacer (A) and textured spacer (D) in the defect site during the “pre-procedure” (Stage 1), the induced membrane four weeks later during the “treatment procedure” (Stage 2) after smooth spacer (B) or textured spacer (E) removal, and after scraping the smooth (C) and textured (F) IM.

MicroCT processing and analysis

High-resolution microCT is the primary outcome measure to characterize the amount and distribution of bone within each defect. Prior to scanning, the nail and screws are carefully removed and replaced with a radiolucent rod and cross-pins to maintain the original length and axial and rotational alignment. After centering in the scanner (Inveon microCT scanner, Siemens Medical Solutions, Knoxville, TN), 441 projection images were acquired at 0.5° increments at 39-μm voxel resolution (80 kVp; 500 μA). Data are reconstructed into 3D volumes using a modified tent-Feldkamp algorithm and calibrated to mg/cm³ of HA using an air/water/hydroxyapatite phantom scanned under the same conditions. Bone threshold is set at 1300 mg HA/cm³ (747 HU). The analyzed volume of interest (VOI) included the 5 cm defect region plus 1 cm of bone proximal and distal to the defect. Each specimen is analyzed with segmentation software developed in-house, in which a 3-dimensional cylindrical “defect template” volume 45 mm in diameter and 70 mm in length is manually positioned to define the boundaries of the VOI. Primary outcome is defined as total bone volume (tBV) in the central 2.5 cm region of the defect, which is the most challenging region to heal. Secondary outcomes are radial percent bone volume (%BV), a summation of circumferential bone volume over the length of the 5cm defect, and angle-moment of inertia in the defect site. Summary data of the pattern and extent of mineralization in the defects in each group are illustrated by projecting %BV versus radial position using a 2D color map ranging from 0% (purple) to 60% (red). The x-axis indicates distance from the center of the medullary canal to the periosteal surface (range = 0-29 mm). The y-axis represents the position in the long axis of the bone (range 0 - 70 mm) including the 5 cm defect plus 1 cm proximally and distally. Mean angle-moment of inertia for each group is also plotted using a 2D color plot color map ranging 0 (dark blue) to 7000 (red) in Hounsfield units (HU)*mm² plotted about the bone circumference in the x-axis and the long bone axis position in the y-axis.

Radiographic Analysis

Fluoroscopic imaging of the tibiae, anterior-posterior (AP) and medio-lateral (ML) projections, are performed after: the spacer procedure (week 0), the graft procedure (week 4), follow-up (week 8). Radiographs are obtained after euthanasia (after soft tissues are removed) 12 weeks after the grafting procedure. The resulting images are ranked from 1 (greatest bone healing) to 20 (no healing) by two independent investigators (senior and junior orthopaedic surgeons) who are blinded to treatment allocation. The highest-ranking sites revealed bony bridging (bone extending the length of the defect with no discontinuity) of all four cortices, followed by bony bridging of three, two, one, or none of the cortices. Among samples that have the same number of bony bridges, the ranking is based on the subjective amount of bone observed.

Histology Analysis

Following microCT data collection, histology and histomorphometry are performed. Each fixed tibia is immersed in dilute HCl (~1 week) and then transferred to a 10% EDTA solution until completely decalcified. Decalcified specimens were embedded in paraffin, trimmed to 7 cm to include the 5 cm defect and 1 cm at either end. The specimens were compared with the corresponding Faxitron radiographs to ensure that the correct tissue area is examined. The specimens are then divided into four 1.75-cm long segments that are then cut in the craniocaudal direction on the mid-sagittal plane to yield medial and lateral halves. Medial halves (each including the anterior and posterior cortices) are processed in paraffin (four blocks/specimen), sectioned at 5- μ m, and stained with hematoxylin and eosin (H&E) and Masson's trichrome. For the histomorphometric analysis (Figure 3), total area of bone in the sections from the two central 1.75-cm blocks (total of 3.5 cm) is measured by tracing the perimeter of each individual focus/area of bone tissue in the section in both anterior and posterior cortices (mm^2) using SPOT basic histomorphometry software (SPOT Imaging, Sterling Heights, MI) and summing the results for each animal.

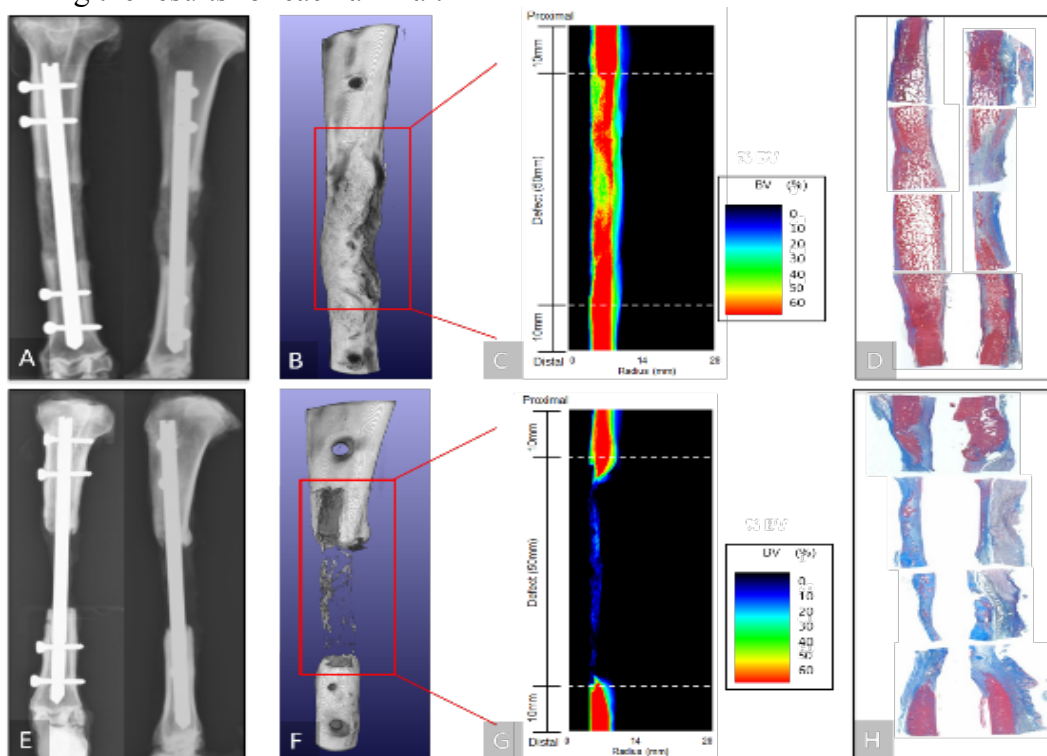


Figure 3 - Postmortem radiographs (AP & ML projections), MicroCT 3D reconstruction, % BV plot vs summation of radial position and Masson's Trichrome stained histology slides for two goats showing robust new bone (pink tissue) formation (A, B, C, D) or minimal new bone formation (E, F, G, H).

Statistical Analysis

All statistical tests are performed using general linear models using one-sided tests at a significance level of 0.05 with SAS 9.4 software (SAS Institute, Cary, NC). The response variable is total bone volume (tBV) in mm³ calculated from the microCT scans in the central 2.5 cm of the defect and the treatment factors are scraped or non-scraped IM and textured or smooth spacers. All data were expressed as mean \pm standard error.

Results:

Three goats were excluded due to complications. Two belonged to the intact/smooth group and were excluded due to Staphylococcus epidermidis infection (n=1) or caseous lymphadenitis (n=1); one goat in the scraped/smooth group was excluded due to anesthetic complication during stage 2 surgery.

Bone formation assessed by MicroCT

Mean percent bone volume in Figure 4 illustrates that there is greater bone formation near the host bone near the osteotomy sites. The angle-moment of inertia plots illustrate that bone tended to form along the posterior and medial aspect of the defect with little bone formation laterally in the IM scraped group while in the intact IM group, new bone formation was found posteriorly. Textured and smooth spacer groups had comparable new bone formation; with bone preferentially forming posteriorly in both groups as shown in the angle-moment plots.

Mean radial tBV in the central 2.5 cm of the defect is significantly greater in the IM scraped group (mean \pm standard error = 1861.0 ± 351.3 mm³) vs. non-scraped IM (930.3 ± 390.3 mm³) (p = 0.041) (Figure 5). However, there was no trend or significant difference between the smooth or textured spacer groups (p = 0.475) (Figure 5). The mean tBV in the central 2.5 cm of the defects was 1413.8 ± 363.3 mm³ for the smooth membrane group and 1377.5 ± 377.5 mm³ for the textured membrane group. These data are graphically presented using a heat map.

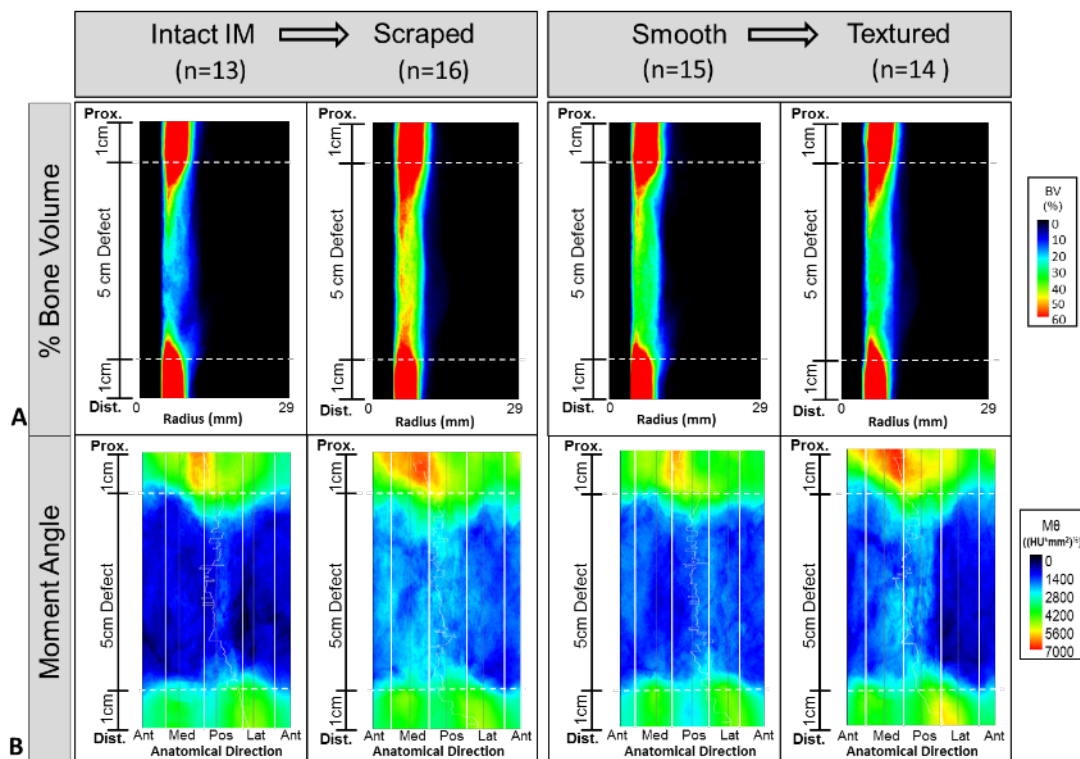


Figure 4 – MicroCT plots illustrating the differences in bone formation and distribution. A) Radial color plot illustrates the probability of bone formation as the summation of the radial location relative to vertical position in the defect. B) Moment-Angle plot illustrates that most bone formed on the posterior aspect of this defect. The proximal and distal borders of the defect are marked by dashed lines.

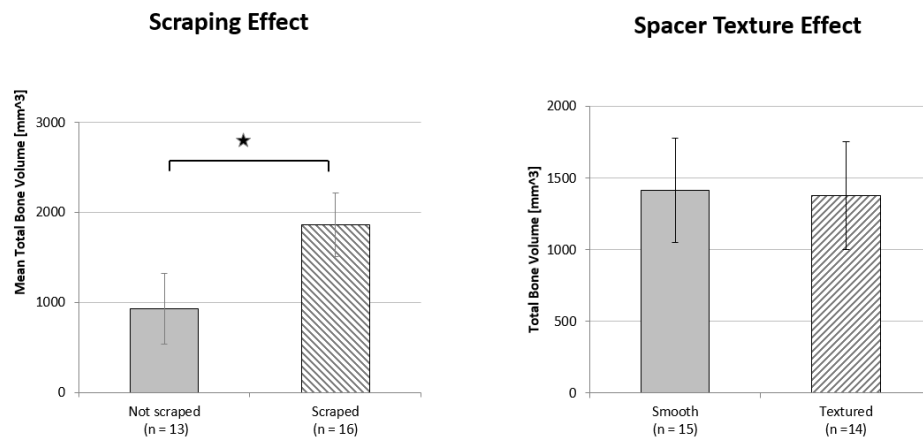


Figure 5 – Total bone volume plots, based on microCT analyses, of the central 2.5 cm of the defect and the entire 5 cm defect illustrating the effect of scraping the IM (A) and the effect of the spacer texture (B).

Postmortem radiograph ranking

Overall, the scraped IM group ranked better than the non-scraped IM group (Figure 6). Ten of the top twelve radiographs belonged to the scraped IM group. The radiographic ranking did not reveal any differences between smooth and textured spacer groups.

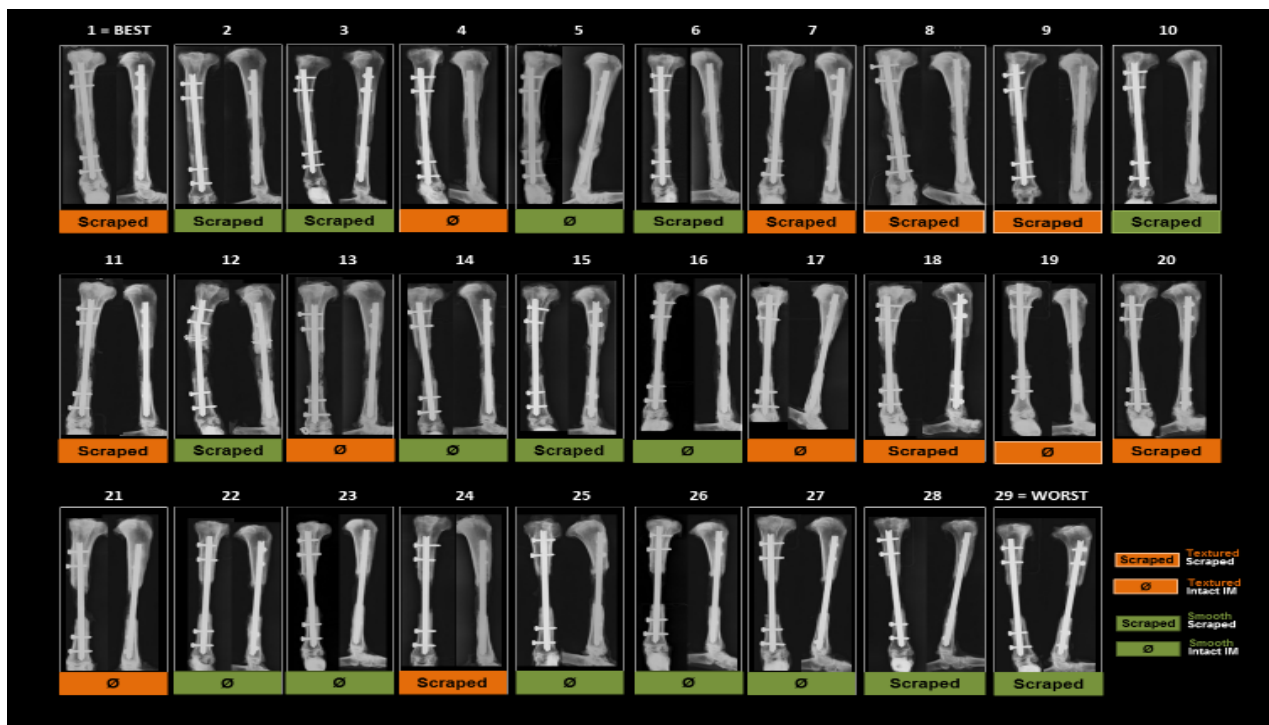


Figure 6 – Postmortem radiographs (AP & ML projections) of the tibia from each goat used for ranking. Higher rank number indicates greater bone formation in the tibial defect (1=complete bone healing; 29=no healing).

Histology

Histological assessment of the goat tibia samples ((Figure 7) identified no evidence of inflammation in any of the sections 12 weeks after grafting. The new bone that was present in the tibias with the most complete healing was similar in quality and was mainly composed of cancellous woven bone. Defects

containing little or no bone were filled primarily with fibrous connective tissue. The most robust bone regeneration occurred in the scraped IM group (mean total bone area = $244.1 \pm 67.8 \text{ mm}^2$) compared to the intact IM group ($177.0 \pm 74.3 \text{ mm}^2$), which is consistent with the microCT data. The histomorphometry data also showed that textured spacer group (mean total bone area = $296.9 \pm 94.3 \text{ mm}^2$) had a larger area of bone in the defect than smooth spacer group ($136.7 \pm 30.4 \text{ mm}^2$). No significant differences were found in histomorphometry assessment between groups.

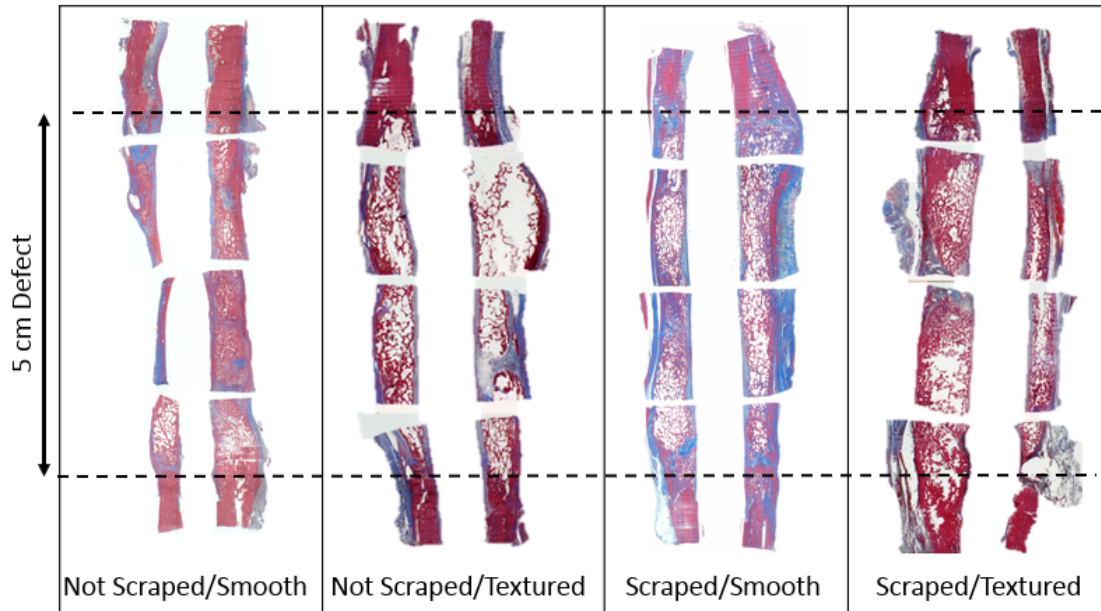


Figure 7 – Histological sections stained with Masson trichrome stain from the tibia from each treatment group that had the greatest bone production. Bone is red and fibrous connective tissue is blue. There were no obvious differences in the quality of the bone tissue; new bone was primarily cancellous woven bone. Tissue in defects with little or no bone was primarily fibrous connective tissue.

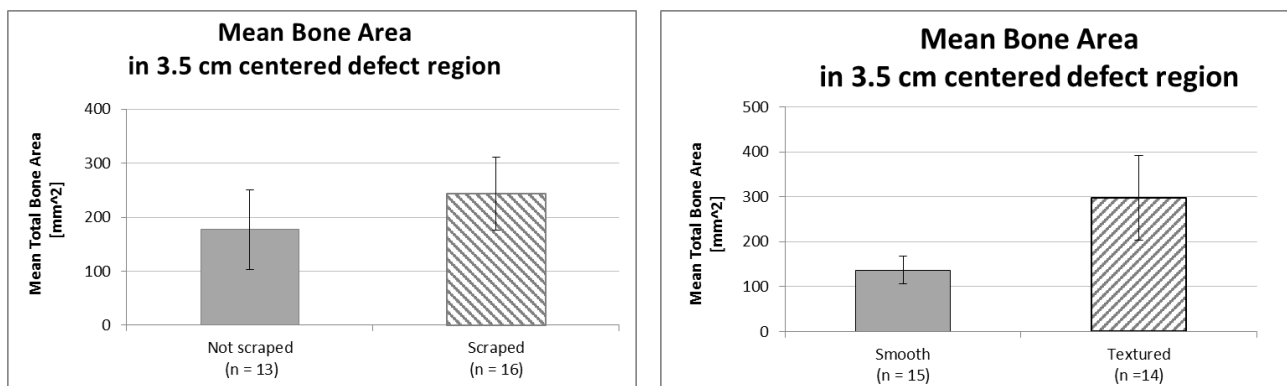


Figure 8 – Histomorphometry data showing no significant differences in bone area vs. treatment.

3.2 Overall Summary for Aim 3:

***Aim 3:** Characterize the histological, biochemical, cellular and gene expression features of the IM and define the features that best predict the magnitude of bone regeneration with ACBG.*

- a) Analysis of autograft cancellous bone graft (ACBG) and bone marrow harvested from sternum

Protocols:

ACBG Histology Protocol: All samples were shipped to the laboratory of Dr. Carlson at University of Minnesota. A 1-cm³ ACBG sample collected for histology analysis was stained with H&E, examined by a board-certified pathologist, and imaged using 1X and 10X objectives. Each sample was characterized by histomorphometry to define areas of hematopoietic marrow, bone, adipose tissue, blood vessels, fibrous tissue, and void spaces. All values are expressed as mean area \pm standard deviation in mm².

Bone Marrow and ACBG Cell/Colony Protocol: All samples were processed in the laboratory of Dr. Muschler at Cleveland Clinic. Marrow (2 cc) was aspirated into a 10-cc syringe containing 1000 U/ml heparin in 0.9% saline (1 cc). ACBG (total volume of 12 cc) was then collected from the 5th sternebra, with additional graft collected from the 4th or 6th sternebra, if needed. Two cell populations were collected from the ACBG sample. Cells that could be mechanically disassociated from the ACBG were defined as marrow space cells (MS) and cells that disassociated only after enzymatic digestion using collagenase I and dispase were defined as trabecular surface cells (TS). Nucleated cells were counted for each sample. The biological performance of osteogenic connective tissue progenitors (CTP-Os) from each sample was assessed using a quantitative colony forming unit assay.

Results:

The ACBG morphology of all goats was similar, with little variation from sample to sample. ACBG histological samples contained abundant bone trabeculae and bone marrow; bone marrow was moderately cellular in all sections. Histomorphometric analysis of the ACBG samples revealed the following percentages of total tissue: hematopoietic marrow = 73.8 ± 14.5 %; bone = 19.6 ± 7.7 %; and hyaline cartilage = 5.8 ± 14.4 %. Blood vessels, fibrous tissue and void spaces were either absent or occupied <1% of the tissue area.

Large variations were seen among animals with respect to cell and CTP-O yield from MS, TS and BM samples, and in the relative distribution of CTP-Os between MS and TS fractions within ACBG samples. Overall, the cellularity in the MS fraction was 2-fold higher than the BM sample and almost 3 fold higher than in the TS fraction (see Table 1). However, the CTP-O prevalence in the TS fraction was approximately 6.5-fold higher than in the MS fraction; and approximately 9-fold higher than BM (see Table 1). We also noted that the total cell count after 6 days in culture was higher in the MS fraction than in the TS fraction, which might indicate that a larger population of cells in the MS fraction were single cells not associated with colony formation.

The yield of cells and CTP-Os, and the associated histology of tissue from the caprine sternum are comparable to human iliac crest; thus this site appears to be suitable for harvest of bone or marrow in this animal model.

These data demonstrate that the overall concentration of CTPs in BM is approximately 5-fold lower than the combined concentration of CTPs in ACBG of comparable volume. This decrease in concentration is due to inefficiency in extraction of the CTP population using simple aspiration and the dilution of the ACBG-derived CTPs with peripheral blood. These data conversely demonstrate that bone marrow processing methods that would increase the concentration of CTPs by just 5-fold would enable a surgeon to transplant a population of cells containing a comparable concentration of CTPs to that in ACBG. These data are exactly analogous to findings demonstrated when comparing human iliac crest core samples with samples of BM from the same iliac crest. These findings suggest that the CCTD model is well suited to further assessment of clinically relevant options to improve the outcome bone regeneration procedures using bone marrow processing.

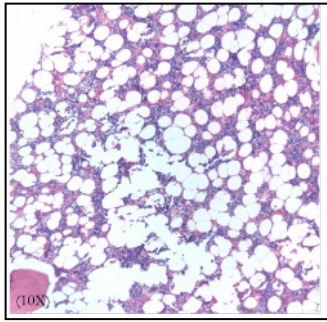


Figure 9- Representative histological image of a caprine sternum ACBG graft showing foci of cancellous bone accompanied by abundant hematopoietic cells (10X; H&E).

	Sternum MS fraction N=32	Sternum TS fraction N=32	Sternum BM N=32
Cells (10⁶/gram or cc)	163.5 ± 11.7 (139.6, 187.4)	56.5 ± 5.9 (44.4, 68.6)	79.4 ± 9.3 (60.4, 98.3)
CTP-O Prevalence (CTPs per 10⁶ cells plated)	56.3 ± 8.6 (38.7, 73.8)	367.7 ± 70.9 (223.04, 512.4)	39.4 ± 5.9 (27.4, 51.5)
[CTP-O] (CTP per gram tissue or aspirate)	8019.0 ± 1393.1 (5177.8, 10860.1)	14167.8 ± 3309.0 (7419.0, 20916.6)	4133.0 ± 923.4 (2249.7, 6016.3)

Table 1. Cell and CTP Yield of MS fraction, TS fraction, BMA. All values are Mean ±SD (Confidence Intervals).

c) Analysis of induced membrane sample

Protocol:

The protocol for sampling the induced membrane harvested using a custom parallel knife instrument at Treatment surgery is illustrated in Figure 10. Data collected from each sample include weight and thickness. Specific segments are analyzed for cells and CTP-Os): (“C”), histology (“H”), and gene expression (“GE”). In the case of “C” and “GE” samples, each segment is divided into an “inner layer” (thin, friable and vascular, immediately adjacent to the spacer) and an “outer” layer (thicker, fibrous, mechanically robust, and less vascular). Samples for cell and CTP analysis are minced and digested in collagenase I and dispase. A standard assay for CTP-Os is performed. Two samples, H2 and H7, were fixed in 10% neutral buffered formalin and transferred to 70% ethanol at 48 hours then shipped to the laboratory of Dr. Carlson at the University of Minnesota for processing. Two samples, GE3 and GE6, were shipped to Dr. Davis at the NMRC for gene expression analysis.

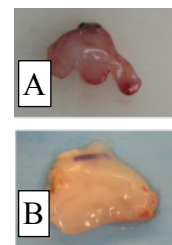
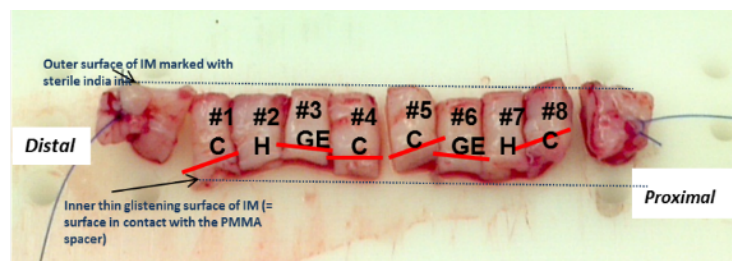
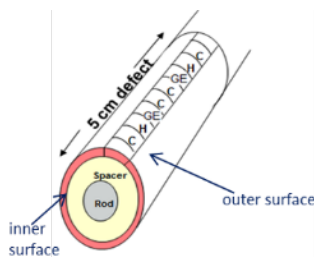


Figure 10 –Induced Membrane sample (7 mm width x 5cm long) excised at the “treatment” surgery. Each strip of IM is sectioned into inner and outer portions for analysis of cells and gene expression (GE3, GE6). The histology sections are kept intact. A) Example picture of a textured induced membrane section; B) Example picture of a smooth induced membrane section picture

Induced membrane histology protocol: All samples were shipped to the laboratory of Dr. Carlson at University of Minnesota. All IM samples were stained with H&E and trichrome stains, examined by a board-certified pathologist, and imaged using a 1X and 10X objective. A grading scheme for the

induced membrane samples has been developed to define overall thickness, cellularity, fibrosis, and vascularity. Grading scheme for induced membrane samples is defined below:

1) If sample contains clearly defined inner and outer zones, measure total thickness in three equidistant sites and express as mean thickness; do not measure samples that appear to have been cut tangentially.

2) Grade the following, on a 0-4 scale:

Fibrosis (on trichrome sections)

- 0 = none
- 1 = < 10% of tissue area is trichrome positive
- 2 = 10-25% of tissue area is trichrome positive
- 3 = >25-75% of tissue area is trichrome positive
- 4 = >75% of tissue area is trichrome positive

Vascularity

- 0 = none
- 1 = minimal (very few vessels present, <5)
- 2 = mild (low numbers of vessels present diffusely throughout the section, 5-10)
- 3 = moderate (contains areas of increased numbers of vessels 9vessel area > tissue area)
- 4 = severe (majority of section contains vessel area that is greater than tissue area)

Cellularity

- 0 = No inflammatory cells
- 1 = Inflammatory cells confined to inner 10% of membrane thickness
- 2 = Inflammatory cells present in 10-25% of membrane thickness
- 3 = Inflammatory cells present in 25-75% of membrane thickness
- 4 = Inflammatory cells present in >75% of membrane thickness

Induced membrane cell/CTP analysis protocol: All samples were processed in the laboratory of Dr. Muschler at Cleveland Clinic. Specific segments were analyzed for cells and osteogenic connective tissue progenitors (CTP) ("C"). Each segment was divided into an "inner layer" (zone immediately adjacent to the spacer) and an "outer" layer. "C" Samples were minced and incubated in 10 ml of prepared digest (collagenase I (111 U/ml) + dispase (24U/ml)) for 1.5 hours at 37° C. Complete media was added to stop digestion, the sample was filtered through a cell strainer, and a cell count was obtained. Cells were cultured at 50 x 10³ cells/chamber for the membranes obtained with smooth spacer (set 1) and 25 x 10³ cells/chamber for the membranes obtained with textured spacer (set 2) in osteogenic media, harvested on day 6. Day 6 cultures were fixed with 1:1 acetone:methanol for 10 min and stained for nuclei (4,6-diamidino-2-phenylindole [DAPI]) and alkaline phosphatase (AP) as a marker for the osteoblastic progenitor activity. Chambers were scanned and analyzed using Colonyze™ software for colony assessment [7].

Induced membrane gene expression analysis protocol:

Induced membranes samples were obtained after a smooth (data set 1) or textured (data set 2) spacer. Sample sections were collected along the tibia shaft either proximally ("6") or distally ("3") from the hip. Both an outer (o) and inner (i) layer of the induced membrane was dissected along with tibial muscle for control tissue and immediately stored in RNAlater at 4°C. Samples were shipped to NMRC (Dr. Davis/Forsberg) for analysis. Total RNA is extracted using the RNeasy Plus Universal Kit (Qiagen, Gathersburg,MD). mRNA quantity and quality are assessed by measuring the A_{260/280} and A_{260/230} ratio with a Nanodrop Spectrophotometer (NanoDrop Technologies Inc., Wilmington,DE) and the 28S/18S rRNA ratio and RNA integrity number (RIN) using an Agilent 2100 BioAnalyzer (Agilent Technologies Inc., Santa Clara, CA). First-strand cDNA is synthesized using the SuperScript III First-Strand Synthesis SuperMix (Life Technologies, Rockville,MD). Quantitative qRT-PCR is performed using the ABI QuantStudio 7-Flex Detection System (Applied Biosystems, Foster City,CA). 18S rRNA, GAPDH and β-actin were used for normalization. The C_t method is used to calculate the relative

expression by $2^{-\Delta\Delta C_t}$ using tibial muscle collected during the defect surgery. For data set 1 (smooth spacer), PCR was conducted on sample of 125 ng of cDNA and for data set 2 (textured spacer), PCR was conducted on sample of 125 ng. After analyzing set 1, the amount of cDNA was considered to be possibly too low. Therefore, in set 2 (textured samples), the protocol was changed to load the PCR reaction with 1 μ g.

Statistical analysis was performed using generalized linear mixed model with Bonferroni correction using SAS 9.4 software (SAS Institute, Cary, NC). The response variable was each gene, the treatments were membrane position (distal vs. proximal) and membrane location (inner vs. outer). The effect of goat was included as a random factor. Statistical significance was determined for $p < 0.0026$.

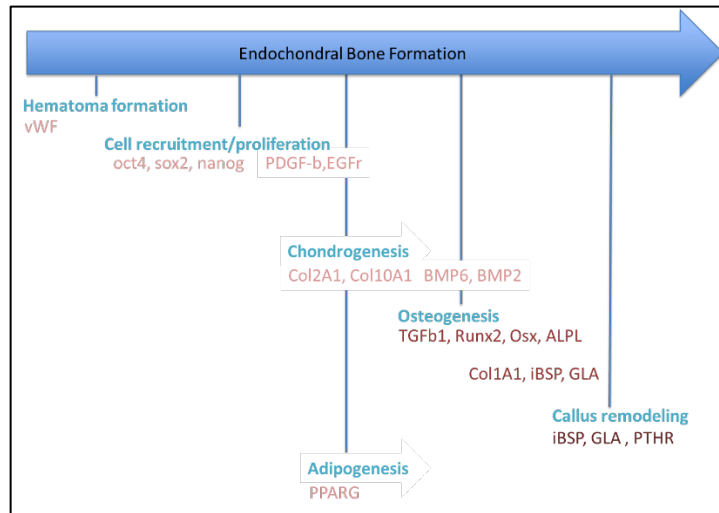


Figure 11 – Genes involved in the endochondral bone repair process

Gene	Function
VWF	Encodes a glycoprotein which functions as an antihemophilic factor carrier and a platelet-vessel wall mediator in the blood coagulation system. It is crucial to the hemostasis process.
OCT4	Encodes a transcription factor containing a POU homeodomain that plays a key role in embryonic development and stem cell pluripotency.
SOX2	Encodes a member of the SRY-related HMG-box (SOX) family of transcription factors involved in the regulation of embryonic development and in the determination of cell fate.
NANOG	Transcription factor involved in maintaining pluripotency in embryonic stem cells.
PDGFB	Protein encoded by this gene is a member of the platelet-derived growth factor family.
EGFR	Encodes a transmembrane glycoprotein that is a member of the protein kinase superfamily. This protein is a receptor for members of the epidermal growth factor family.
COL2A1	Encodes the alpha-1 chain of type II collagen, a fibrillar collagen found in cartilage.
COL10A1	Encodes the alpha chain of type X collagen, a short chain collagen expressed by hypertrophic chondrocytes during endochondral ossification.
BMP6	Part of a family of secreted signaling molecules that can induce ectopic bone growth. This gene has a proposed role in early bone development.
BMP2	Encodes a protein that acts as a disulfide-linked homodimer and induces bone and cartilage formation.
TGFB1	A polypeptide member of the transforming growth factor beta superfamily of cytokines.
RUNX2	Essential for osteoblastic differentiation and skeletal morphogenesis and acts as a scaffold for nucleic acids and regulatory factors involved in skeletal gene expression.
OSTERIX	Bone specific transcription factor that is required for osteoblast differentiation and bone formation.
ALPL	Encodes a membrane bound glycosylated enzyme, a proposed function of this form of the enzyme is matrix mineralization.
COL1A1	Encodes a fibril-forming collagen that is found in most connective tissues and is abundant in bone, cornea, dermis and tendon.
IBSP	Protein encoded by this gene is a major structural protein of the bone matrix
GLA	Encodes a homodimeric glycoprotein that hydrolyses the terminal alpha-galactosyl moieties from glycolipids and glycoproteins.
PTHr	A member of the G-protein coupled receptor family 2 that is a receptor for parathyroid hormone (PTH) and for parathyroid hormone-like hormone (PTHrP).
PPARG	Protein encoded is a regulator of adipocyte differentiation.

Table 2. Gene Analysis in Goat Induced Membranes.

Results:

Histology Results (Figure 12): All IM samples had a similar appearance in each treatment groups. Each IM sample included two relatively distinctive layers. Immediately adjacent to the spacer, a narrow inner zone was composed of dense mononuclear cells that appeared to be composed primarily of macrophages (foreign body response) with rare inflammatory cells. Variable numbers of small-caliber blood vessels were also present in the inner zone. The remainder of the tissue (outer section) was composed of fibrous connective tissue that extended to the deep margin of the section. All samples exhibited diffuse trichrome positivity indicative of the presence of fibrous connective tissue.

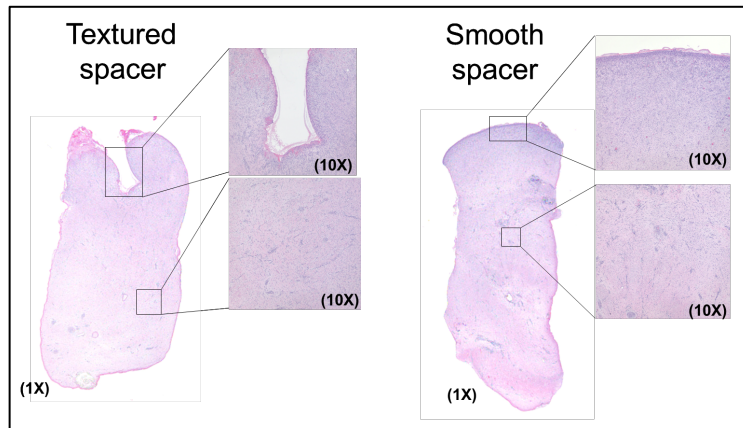


Figure 12 – Example of IM histology slide stained with H & E in textured spacer group and the smooth spacer group.

Cell/CTP analysis Results:

	Smooth Spacer		Textured Spacer	
	Inner IM N= 12	Outer IM N=12	Inner IM N= 16	Outer IM N=16
Cell Yield (Million cells per gram)	25.4 ± 5.5	11.2 ± 2.4	14.9 ± 1.8	6.9 ± 1.1
Total cell count after 6 Day culture (cells per cm ²)	4043.4 ± 1336.7	3662.0 ± 1272.1	5441.5 ± 1275.9	5272.1 ± 1015.2

Table 3 - Cellularity, total cells after 6 days in culture in each group. Data are expressed as mean ± standard deviation.

Cellularity:

The number of nucleated cells per gram of digested membrane tissue varied significantly between smooth and texture groups as shown in Table 3. Mean inner membrane cellularity for smooth spacer group was $25.6 \pm 18.7 \times 10^6$ cells per gram and $14.9 \pm 7.0 \times 10^6$ cells per gram for the textured spacer group. Mean outer membrane cellularity for smooth spacer group was $11.2 \pm 8.5 \times 10^6$ cells per gram and $6.8 \pm 4.5 \times 10^6$ cells per gram for the textured spacer group.

The smooth spacer group had statistically significantly higher number cells per gram than textured membrane group for both inner and outer membranes.

Inner IM samples had significantly higher cell yield per gram than the outer IM by approximately two-fold in both smooth and textured spacer groups (Table 3).

Colony:

Both inner and outer IM samples cultured in osteogenic differentiation media at Day 6 showed confluent colonies for most samples with large numbers of free cells and development of nodular structures, which appeared as highly dense, multi-layer clusters of cells. Therefore, no CTP Prevalence was obtained; only CTP progeny cell count at Day 6 was measured. These nodules were also found to be mineralized as demonstrated by positive alizarin red staining, a technique commonly used to detect calcium deposition in osteoblast cultures.

The number of CTP progeny cells at Day 6 varied significantly among samples. Mean inner membrane CTP progeny cells at Day 6 for the smooth spacer group was 4043.4 ± 1336.7 cells per cm^2 and 5441.5 ± 1015.2 cells per cm^2 for the textured spacer group. Mean outer membrane CTP progeny cells at Day 6 for the smooth spacer group was 36262.0 ± 1275.9 cells per cm^2 and 5272.1 ± 1015.2 for the textured spacer group. CTP progeny cell at Day 6 were comparable for both inner and outer samples. There was a trend for higher CTP progeny cell count at Day 6 in the textured spacer group than in the smooth spacer group but this difference did not reach significance.

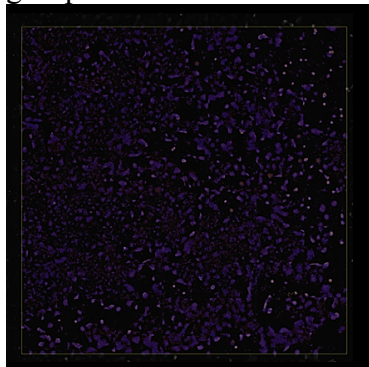
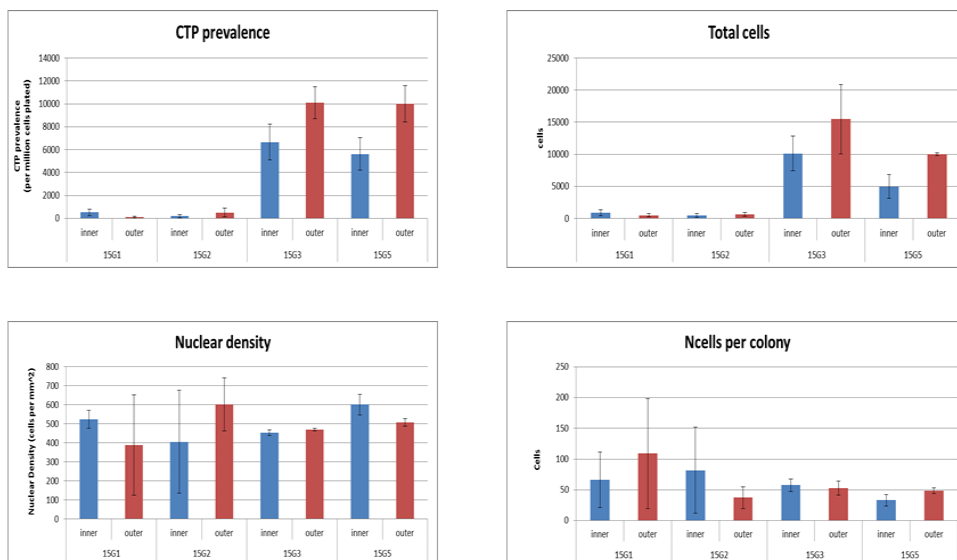


Figure 13 – Representative example of IM cell culture chambers at Day 6 showing many cells and confluent colonies.

For 4 goats, we were able to measure colony count at Day 6. The results are reported in Figure 14 below. Based on the 4 goats where we were able to count colonies, we measured that mean CTP Prevalence was 4214.24 ± 4409.85 colonies per $\times 10^6$ cells plated. The number of cells per colony and colony size for goat membrane samples was highly variable, 1 colony can contain between 13 and 213 cells. Similar findings are also found in human iliac crest bone marrow aspirate samples.

COLONYZE output Summary for 4 goats



*Average was calculated with median \pm standard deviation

Figure 14 – CTP Prevalence, nuclear density, cells per colony, total cells at Day 6 within chambers for the four goats with countable colonies.

The induced membrane has biological characteristics and properties that may be used for improving the outcome of bone tissue engineering purposes. However, the cell plating density remains to be optimized for colony analysis. Further studies are still needed to optimize the osteogenic features of the induced membrane. We recommend a lower plating density of 10,000 cells per chamber (5,000 cells/ml) is now recommended for future studies so further characterization of the induced membrane can be made.

Gene expression Results:

Data set 1 (Figure 15) showed more variation that might reflect problems when processing these samples. The low amount of cDNA (125 ng) used to load per plate might have been too low resulting in non-detectable levels of some genes and therefore led to greater variations in the data. Data Set 1 are reported here but no conclusive analysis was drawn from this set. Conclusions were only made on the analysis of set 2 (textured spacer) (Figure 16).

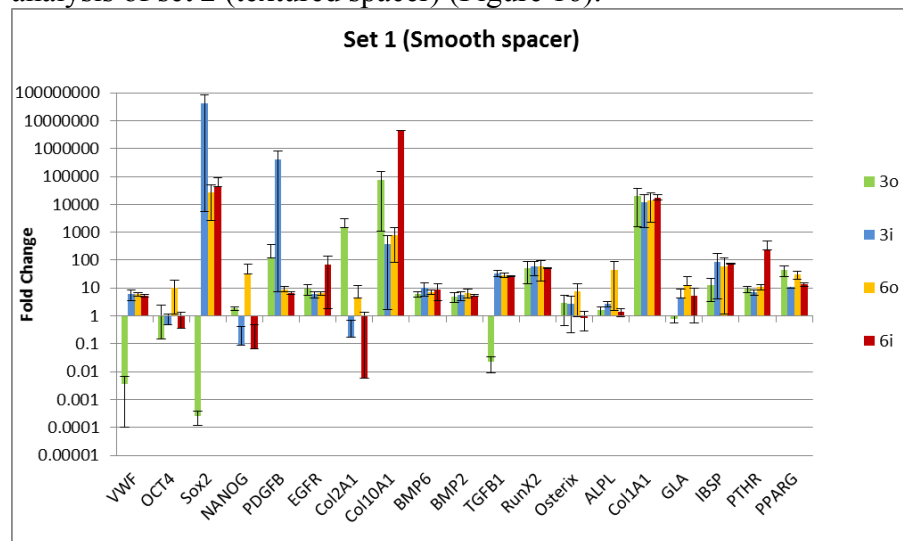


Figure 15 - Gene expression of membrane sections normalized to goat muscle after smooth spacer implantation (Set 1). Each bar represents mean fold change \pm standard deviation.

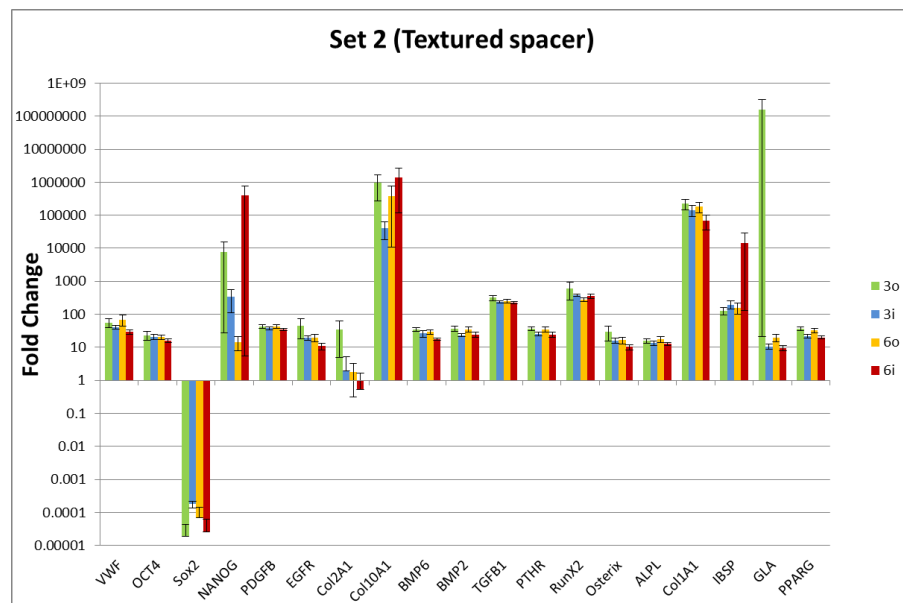


Figure 16 – Gene expression of membrane sections normalized to goat muscle after textured spacer implantation (Set 2). Each bar represents mean fold change \pm standard deviation.

Comparison IM vs. Muscle (Table 4): The gene expression analysis from Data set 2 (texture surface) was loaded with 250 ng cDNA. These data demonstrated less variation than set 1. These data showed

upregulation of target genes relative to normal muscle, with the one exception of Sox2 (gene involved in cell fate), which was decreased by approximately 210-fold.

13 of 19 genes of IM samples were significantly different than normal muscle. These included RunX2, Osterix, PPARG, OCT4, ALPL, EGFR, VWF, PDGFB, TGFB1, BMP2, BMP6, Col1A1, PTHR. We noted that Col1A1 gene fold change was significantly high (95% Confidence Interval after Bonferroni correction was 76600 to 241500 fold). RunX 2 and TGFB1 genes had a fold change in the order 100 fold. All other genes had moderate increase (less than 35 fold). These results indicated evidence of genes within the IM cell population that have osteogenic and chondrogenic potential.

Set 2 = Textured							
	Mean Fold change (including all inner, outer, distal, proximal)	Median	SD	SE	SE after Bonferroni correction	Significance (adjusted after Bonferroni) Confidence interval lower limit	Confidence interval upper limit
VWF	50.9	35.1	60.4	7.8	21.8	29.2	72.7
OCT4	20.0	14.4	16.7	2.2	6.0	14.0	26.0
Sox2	-32371.3	-209.7	109064.8	14080.2	39283.7	-71655.1	6912.4
NANOG	93373.3	5.5	707543.3	91343.4	254848.1	-161474.8	348221.4
PDGFB	38.6	36.4	16.6	2.1	6.0	32.6	44.5
EGFR	25.1	12.6	56.8	7.3	20.5	4.6	45.5
Col2A1	8.4	-1.2	57.3	7.4	20.6	-12.2	29.0
Col10A1	1020688.3	62.1	3805525.9	491291.1	1370702.1	-350013.8	2391390.4
BMP6	27.0	23.0	18.0	2.3	6.5	20.5	33.5
BMP2	29.5	25.8	19.8	2.6	7.1	22.4	36.7
TGFB1	259.7	224.3	145.4	18.8	52.4	207.4	312.1
PTHR	29.7	24.5	19.5	2.5	7.0	22.6	36.7
RunX2	411.9	297.6	671.7	86.7	241.9	170.0	653.8
Osterix	18.4	13.7	28.8	3.7	10.4	8.0	28.8
ALPL	15.1	12.6	10.0	1.3	3.6	11.5	18.7
Col1A1	159024.6	23339.7	228951.1	29557.4	82465.3	76559.3	241489.9
IBSP	3488.1	91.1	25804.4	3331.3	9294.4	-5806.3	12782.5
GLA	39695877.8	9.9	307482829.5	39695845.6	110751409.3	-71055531.5	150447287.1
PPARG	26.9	22.8	16.5	2.1	5.9	21.0	32.9

Table 4 - Summary of overall statistical analysis of genes in the IM compared to muscle. Genes that showed significant difference with fold change <2 but <35 are highlighted in yellow; with fold change >150 but <500 in orange, and >50,000 fold change in purple.

Comparison between proximal and distal samples (Table 5): No significant main effects were found for target gene fold-change between distal or proximal sections in the data set 2.

Set 2 = Textured						
	Distal Mean Fold change	SD Inner	Proximal Mean Fold change	SD Outer	Mean Difference (Distal - Proximal)	p value
VWF	48	48.7	53.9	71	-5.9	0.645
Oct4	21.7	21	18.3	11	3.4	0.3892
Sox2	-35005.6	131265.3	-29737.1	83399.5	-5268.5	0.8564
NANOG	4020.7	21012.8	182725.8	1000768.6	-178705.1	0.3311
PDGFB	39	16	38.1	17.3	0.9	0.8227
EGFR	32	78	18.1	19.5	13.9	0.3228
Col2A1	16.7	80.7	0.1	4.8	16.6	0.2037
Col10A1	682733.9	2144518.9	1358642.7	1020688.3	-675908.8	0.72228
BMP6	29.7	21.2	24.3	14.1	5.4	0.2297
BMP2	29.3	20.2	29.7	19.8	-0.4	0.9303
TGFB1	265.9	169.4	253.6	119.4	12.3	0.695
PTHR	29.9	17.8	29.4	21.4	0.5	0.9134
RunX2	491.1	934.9	332.7	175.5	158.4	0.3542
Osterix	22.8	38.6	14	12.7	8.8	0.2147
ALPL	14.3	9	15.9	11	-1.6	0.4611
Col1A1	182452.2	252952.2	135596.9	203775.4	46855.3	0.1334
IBSP	172	172.2	6804.2	36495.4	-6632.2	0.3257
GLA	79391740.6	434846388	15.1	14.7	79391725.5	0.3237
PPARG	28	16.3	25.9	16.9	2.1	0.5698

Table 5 - Summary of overall statistical analysis of IM gene fold change comparing distal to proximal sections. There were no significant differences between distal and proximal for any gene.

Comparison between inner sections and outer sections (Table 6): The data analysis of set 2 showed that gene expression in the inner surface (1 mm) of the IM differs from the rest of the IM. Overall, the fold change in the inner samples was lower than in the outer sample.

No significant differences between inner and outer sections were detected after the Bonferroni adjustment except for PPARG. The fold change for PPARG (involved in adipocyte differentiation and decrease of anti-inflammatory response) in the inner sample was approximately 14.7-fold lower than the outer sample ($P=0.0011$). Five genes, TGFB1, BMP2, BMP6, Col1A1 and PTHR, showed trends that approached a significant difference, with values of fold change that were lower in the inner layer of the IM than in the outer layer. These genes are all considered to be pro-osteogenic. It is therefore possible to speculate that the removal of the inner-most layer of the IM where these genes were expressed at lower levels may be a mechanism that contributes to the finding of increased bone formation in the scraped IM defect sites.

Set 2 = Textured						
	Inner Mean Fold change	SD Inner	Outer Mean Fold change	SD Outer	Mean Difference (Inner - Outer)	p value
VWF	35.6	20.5	66.3	80.8	-30.7	0.0271
Oct4	18.8	11.4	21.2	20.9	-2.4	0.5464
Sox2	-25942.0	96710.2	-38800.7	121499.1	12858.7	0.6596
NANOG	182885.2	1000738.7	3861.3	21033.7	179023.9	0.3302
PDGFB	35.1	11.6	42.0	20.0	-6.9	0.0818
EGFR	14.9	11.4	35.3	78.9	-20.4	0.1563
Col2A1	-1.2	3.1	18.0	80.5	-19.2	0.2682
Col10A1	847749.0	3392663.0	1193627.7	4229822.0	-345878.7	0.4909
BMP6	21.3	16.4	32.8	18.0	-11.5	0.0189
BMP2	23.1	11.3	35.9	24.2	-12.8	0.0099
TGFB1	219.9	54.2	299.6	191.9	-79.7	0.0214
PTHR	23.3	14.1	36.0	22.2	-12.7	0.0076
RunX2	365.0	164.2	458.8	941.5	-93.8	0.5793
Osterix	13.7	9.4	23.2	39.4	-9.5	0.1808
ALPL	13.4	7.2	16.7	12.1	-3.3	0.1383
Col1A1	115731.9	175080.7	202317.2	268540.0	-86585.3	0.0107
IBSP	6841.5	36488.3	134.7	180.7	6706.8	0.3205
GLA	9.8	5.8	79391745.8	434846387.0	-79391736.0	0.3237
PPARG	19.6	8.3	34.3	19.3	-14.7	0.0011

Table 6 - Summary of overall statistical analysis of IM gene fold change comparing inner sections to outer sections. Genes that showed significant difference with $p > 0.0026$ are highlighted in green; those with a trend for difference ($0.0026 < p < 0.05$) are highlighted in yellow.

c) Predictive modeling (NMRC)

Protocol:

Data preprocessing -

- Missing data:** Most modeling algorithms fail when the data contains missing values; one exception to that are Bayesian based algorithms. The data collected was missing around 1% of values that were imputed using missForest, used to impute missing values particularly in the case of mixed-type data, in R. It can be used to impute continuous and/or categorical data including complex interactions and nonlinear relations. It yields an out-of-bag (OOB) imputation error estimate [8].
- Formatting the variables:** In order to run logistic regression on the scraping variable and spacer texture, data were converted to factor with 2 levels: 0 and 1. The data were partitioned between training and test set in a proportion of 70% and 30%, respectively. The small sample size of 32 compelled us to test the model with a 50:50 proportion.
- Modeling the effects of spacer texture on collected:** Setting spacer texture as the response variable, a naïve Bayesian based model was built on the training data. The standard naive Bayes classifier relies on the assumption of independence of the predictor variables, and of metric predictors that are normally distributed (Gaussian). Sensitivity and specificity tests were performed on the model performance to discriminate between spacer textures. Individual experiments were modeled to see their effects on spacer texture. Logistic regression was done for numerical data, and variables with a significant P value were retained for model building.

1. **Effects of spacer texture on CT-2.5 level (i.e. total bone volume in 2.5 cm central region) and X-Ray values:** A logistic regression modeling was performed to look at the effects of spacer texture and membrane scraping on CT-2.5 and X-ray values.
 2. **Effects of spacer texture in predicting IM Biology:** The effects of nine biological metrics to predict spacer texture were analyzed using a logistics regression technique (Table IM Biology). Variables with a p-value < 0.05 were considered significant in predicting spacer texture.
 3. **Effects of spacer texture on gene expressions in the inner section:** The expression of nineteen genes located in the inner IM section were investigated in relation to spacer texture using logistic regression. Important genes expressed due to spacer texture were selected in model building (gene expression table). Due to the quality of the data which appeared unscaled and impossible to analyze by logistic regression, we resolved to select by other methods the top variables important in building model around the spacer texture. Random forest based model was built to select important genes for predictive modeling. Random forest is primarily an ensemble learning method for classification and regression (**Brenan**). Others model building techniques such as **Boruta** [9], **Lasso** [3], **pda** PDA (penalized discriminant analysis), **nnet** (Neural network) were run to select important genes. Important variables returned will be used to build final model. Boruta is an R package that acts as a wrapper algorithm for relevant feature selection. It finds important variables by comparing original attributes importance with the importance achievable at random, estimated using their permuted copies and progressively eliminating irrelevant features to stabilize the test. By default, Boruta uses random forest for computing. Lasso is a shrinkage and selection method for linear regression. It minimizes the usual sum of squared errors with a bound on the sum of the absolute values of the coefficients. It is considered more stringent than logistic regression. PDA (penalized discriminant analysis) is a data analytic tool for studying the relationship between a set of predictors and a categorical response. It is used in cases where there are many highly correlated predictors. It is also used for dimension reduction. Nnet (Neural network), used in the R package, is a feed-forward neural network with a single hidden layer.
 4. **Effects of spacer texture on gene expressions in the outer section:** The same analysis pathway used to select important genes expressed will be applied to genes expressed in the outer section.
- d) **Modeling the effects of membrane scraping on outcome variables:** The same approach to feature selection that was applied to spacer texture was used in modeling for membrane scraping.
 - e) **Predictive modeling of the effects of IM biology on microCT-2.5 level (i.e. total bone volume in 2.5 cm central region):** Direct linear effect of scraping on the level of CT-2.5 was investigated. A linear regression equation was designed to answer to question of any potential relation between scraping and CT-2.5 level.
 - f) **Effects of gene expression in the inner and outer section on the microCT-2.5 level:** A linear regression model was designed to select the genes that were significantly expressed in relation to CT 2.5 level.
 - g) **Effects of graft, cellularity on microCT-2.5 level:** Linear regression equations were generated to model the contributions of ACBG and IM cellularity variables on CT-2.5 level. Features that contributed significantly to CT-2.5 level were retained in the final predictive model.

Data Modeling Protocol –

A table containing a total of 32 observations of data collected from various experiments were pooled in a spreadsheet. It contained data on goat (age, weight), data on the surgeon who performed the surgeries, the quantitative histology of the IM tissues graft, the quantitative histology of the tibia defect, the expression profiles of 19 genes in the inner and outer membrane sections, the CT scan of the tibia defect, and the X-ray healing ranking. The data were organized to match each goat for easy analysis. The

animals age ranged from 3 to 5 years, and weight from 41-65 kg. Four different surgeons dissected, scraped the membrane and implanted the spacers in the animals. Goats that were grouped as membrane scraped or not (0, for not scraped and 1 for scraped), and spacer texture. Sixty-nine features were collected from the 32 goat in the study for a total of 2208 data entries in the database. Of the 2208 data collected, 8 were missing which were subsequently imputed using missForest algorithm. The table contained mixed data types: integers, numerical, and factor.

- a) **Predicting microCT total bone value from the predictors collected:** A regression analysis using microCT-2.5 values as the response variable from the experiments performed on the goats was done. Due to the various data structure, we grouped the data by experimental type:
- Group 1 included scraping parameter, spacer texture parameter, microCT-5 values (i.e. total bone volume in 5 cm defect region), and X-Ray healing rank.
 - Group 2 comprised of the IM histology features (Tib histo bone area, IM histo vascularity, IM histo fibrosis, IM histo inflammatory cellularity, IM histo thickness, IM membrane weight, IM inner mean cellularity, and expanded IM inner cells).
 - Group 3 was the genes located in the inner section of the membrane tested.
 - Group 4 comprised genes located on the outer section of the membrane
 - Group 5 comprised ACBG and BM biology parameters. The variable included in the model building were BM CTP prevalence, MS cellularity, MS CTP prevalence, TS cellularity, TS CTP prevalence, MS CTP prevalence, graft histo cartilage, graft histo bone, graft histo hematopoietic marrow, graft histo adipose tissue, and graft histo vasculature area.
- b) **Effects of spacer texture and membrane scraping on microCT-2.5 level and X-ray healing rank:** We wanted to know if spacer texture and membrane scraping could predict microCT-2.5 level and X-ray healing rank. The response variable membrane scraping and spacer texture are both binary outputs so we ran logistic regression models.
- c) **Effect of spacer texture on IM biology.**

Results:

1. Data compiled from the IM goat study

The code ran in 0.24 seconds. After the missing data were successfully imputed, modeling could be performed. The total observations were partitioned 70% for training data and 30% for testing the model. The partition were achieved using the function create partition from the caret packages in R which splits the data 24 observations for building the model and 8 for testing its predictive performance.

2. Building a classification model around the spacer texture and membrane scraping.

Can all the features measured help sort out goats based on spacer texture? Seventeen (17) goats had spacer texture and 15 did not. In order to answer this question, and naïve Bayes function was run on the whole data. The model was sensitive at 93%, 100% specific, and PPV was 100% and NPV was 94.4%. Of the 8 test data, 4 were grouped as 0, and 3 as 1.

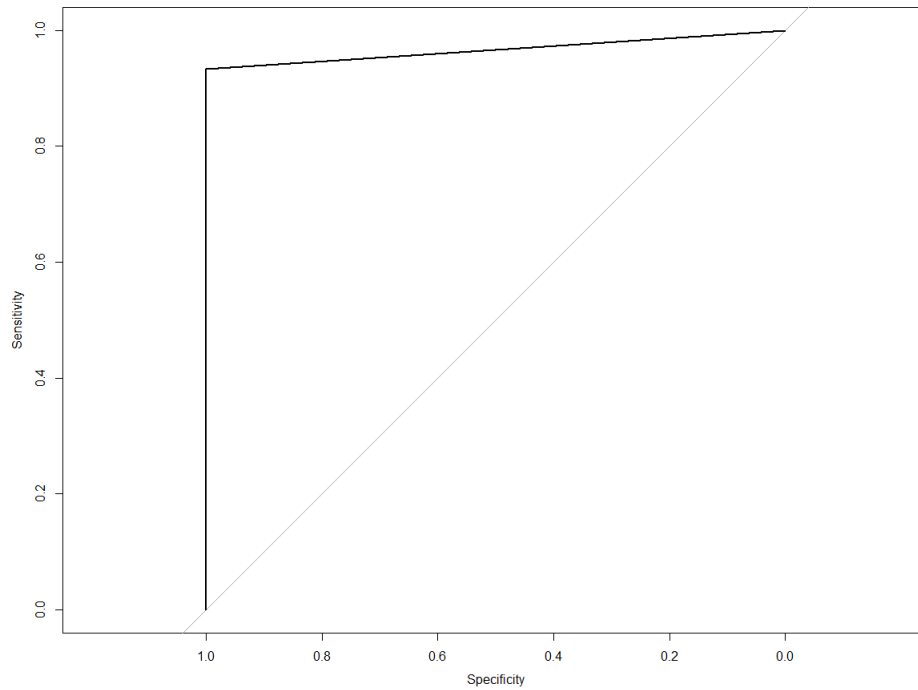


Figure 17 – ROC curve for spacer texture model: The model using all observed predictors was 93% sensitive and 94% specific.

Of the 32 observations, 16 had scraped membranes and 16 not scraped. Using all the features collected, we built a predictive tool to predict goats with scraped membranes. The model performed at 100% sensitivity and 54% specificity for PPV of 70% and NPV of 100%.

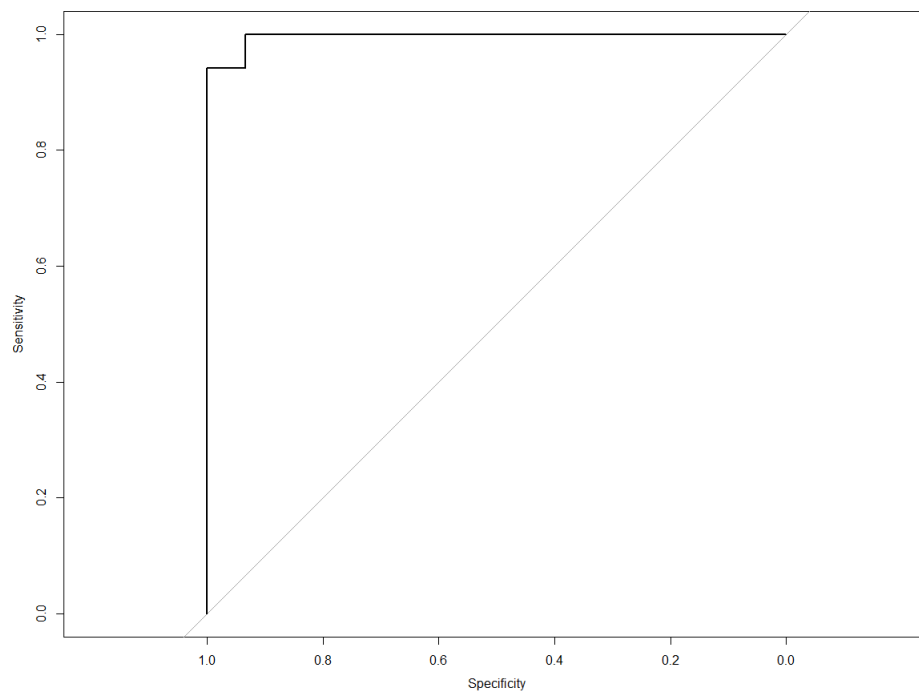


Figure 18 – ROC curve for membrane scraping model. The model performed at 100% sensitivity and 54% specificity for PPV of 70% and NPV of 100%.

3. Predicting microCT scan value from the predictors collected

Regression analysis using microCT-2.5 (total bone volume in 2.5 cm central region) values as the response variable from the experiments performed on the goats was done. Due to the various data structure, we grouped the data by experimental type.

The first group included scraping, spacer texture, microCT-2.5, microCT-5, and X-Ray healing rank. The model looked at these variables to predict microCT-2.5. We found that microCT.5 (total bone volume in 5 cm defect region) was a better predictor of microCT-2.5 values at the p value = 1.9e-15.

Estimate	Std.	Error	t-value	Pr(> t)
(Intercept)	-192.636	255.3244	-0.754	0.457
scraping1	20.13033	70.2536	0.287	0.777
Spacer.texture1	54.75502	69.36942	0.789	0.437
CT.5	0.49048	0.03024	16.222	1.90E-15
Xray.Rank	-5.33292	9.86053	-0.541	0.593

Table 7 - Linear regression metrics for microCT-2.5 model for group 1.

Group 2 comprised of the IM histology features (tibial histology bone area, IM histology vascularity, IM histology fibrosis, IM histology inflammatory cellularity, IM histology thickness, IM membrane weight, IM inner mean cellularity, and Day 6 IM inner and outer cell count). We found tibia histology bone area to be a more significant predictor (p= 0.00762) of microCT-2.5 level than the other features tested in group 2.

	Estimate	Std. Error	t value	Pr(> t)
(Intercept)	-1.195e+03	6.455e+03	-0.185	0.85491
Tib_Histo_Bone.Area..3.5	2.927e+00	9.918e-01	2.952	0.00762
IM_Histo_Vascularity	-4.847e+02	5.613e+02	-0.863	0.39763
IM_Histo_Fibrosis	1.930e+02	1.640e+03	0.118	0.90746
IM_Histo_inflammatory_Cellularity	-8.182e+02	6.398e+02	-1.279	0.21493
IM_Histo_Thickness	1.578e+02	1.238e+02	1.275	0.21627
IM.membrane.__.weight	2.750e+03	3.529e+03	0.779	0.44450
IM_Inner.Mean.cellularity	1.916e+01	1.772e+01	1.081	0.29188
Day 6.IM_inner.cells	7.688e-03	6.773e-02	0.114	0.91070
IM_Outer.Mean.cellularity	-5.130e-01	4.730e+01	-0.011	0.99145
Day 6.IM_outer.cells	2.911e-02	8.575e-02	0.339	0.73763

Table 8 - Linear regression metrics for microCT-2.5 model for group 2.

Group 3 were the genes located in the inner section of the induced membrane (IM). A regression analysis was performed to find which genes significantly predicted microCT-2.5 level. Of the nineteen genes located on the inner IM section, none were significant predictors for microCT-2.5 level.

Coefficients:				
	Estimate	Std. Error	t value	Pr(> t)
## (Intercept)	1.205e+03	1.398e+03	0.862	0.406
## IM_inner_RunX2	3.372e+00	9.111e+00	0.370	0.718
## inner_Osterix	1.234e+01	1.539e+02	0.080	0.937
## inner_PPARG	-3.123e+01	6.238e+01	-0.501	0.626
## inner_OCT4	1.001e+02	8.139e+01	1.230	0.242
## inner_Sox2	3.395e-06	4.176e-06	0.813	0.432
## inner_NANOG	-3.883e-05	8.662e-04	-0.045	0.965

## inner_ALPL	3.089e+01	9.808e+01	0.315	0.758
## inner_EGFR	2.828e+00	2.711e+00	1.043	0.317
## inner_VWF	-9.562e+01	6.040e+01	-1.583	0.139
## inner_PDGF	-2.011e-03	4.525e-03	-0.444	0.665
## inner_TGFB1	-1.727e+00	8.247e+00	-0.209	0.838
## inner_BMP2	8.455e+01	5.804e+01	1.457	0.171
## inner_BMP6	-5.809e+01	5.965e+01	-0.974	0.349
## inner_Col1A1	5.292e-03	7.370e-03	0.718	0.486
## inner_Col2A1	-9.295e+01	1.080e+02	-0.861	0.406
## inner_Col10A1	1.693e-04	3.938e-04	0.430	0.675
## inner_GLA	-6.706e+01	1.179e+02	-0.569	0.580
## inner_IBSP	-2.056e-02	2.162e-02	-0.951	0.361
## inner_PTHR	6.494e+00	5.859e+00	1.108	0.289

Table 9 - Linear regression metrics for microCT-2.5 model for group 3.

Group 4 comprised genes located on the outer section of the IM. A regression model to predict the expression of the genes in response of microCT-2.5 level revealed that five genes were impacted by microCT-2.5. Increased expression of Col1A1 ($p=0.0354$) and BMP2 ($p=0.0264$) had a positive effect on microCT2.5, while Sox2 ($p=0.0860$), BMP6 ($p=0.0557$), Col10A1 ($p=0.0894$) and GLA ($p=0.0764$) approached significance. However, increased expression of BMP6 and GLA were associated with decreased microCT-2.5 level.

## Coefficients:				
##	Estimate	Std. Error	t value	Pr(> t)
## (Intercept)	1.218e+03	6.995e+02	1.741	0.1072
## outer_RunX2	1.646e+00	6.573e+00	0.250	0.8065
## outer_Osterix	4.684e+01	1.013e+02	0.462	0.6521
## outer_PPARG	1.369e+01	1.564e+01	0.876	0.3985
## outer_OCT4	-8.033e+00	6.071e+01	-0.132	0.8969
## outer_Sox2	9.735e-03	5.205e-03	1.870	0.0860 .
## outer_NANOG	1.826e-02	3.739e-02	0.488	0.6342
## outer_ALPL	-1.546e+01	1.476e+01	-1.048	0.3155
## outer_EGFR	-4.765e+01	6.237e+01	-0.764	0.4596
## outer_VWF	2.579e+00	2.173e+00	1.187	0.2583
## outer_PDGF	-4.273e-01	8.039e-01	-0.532	0.6048
## outer_TGFB1	-8.250e+00	8.098e+00	-1.019	0.3284
## outer_BMP2	1.070e+02	4.228e+01	2.530	0.0264 *
## outer_BMP6	-9.506e+01	4.487e+01	-2.119	0.0557 .
## outer_Col1A1	6.920e-03	2.919e-03	2.371	0.0354 *
## outer_Col2A1	1.138e-01	1.150e-01	0.990	0.3417
## outer_Col10A1	4.974e-04	2.692e-04	1.848	0.0894 .
## outer_GLA	-4.847e-06	2.500e-06	-1.939	0.0764 .
## outer_IBSP	2.194e+00	6.783e+00	0.323	0.7519
## outer_PTHR	2.232e+00	4.402e+01	0.051	0.9604

Table 10 - Linear regression metrics for microCT-2.5 model for group 4.

Group 5 investigated the effects of graft biology on microCT-2.5 response. The variable included in the model building were bone marrow (BM) cellularity and CTP prevalence, Marrow Space (MS) cellularity

and CTP prevalence, Trabecular Surface (TS) cellularity and CTP prevalence, ACBG histology cartilage area, graft histology bone area, graft histology hematopoietic marrow area, graft histology adipose tissue area, and graft histology vasculature area.

The features that were significant predictors of microCT-2.5 level were CTP prevalence for Trabecular Surface of ACBG graft ($p=0.00424$) and near significant features were CTP prevalence of bone marrow ($p=0.07547$), and ACBG histology adipose tissue amount ($p=0.08598$). Note that the effect of ACBG adipose tissue was negative, therefore increasing adipose histology was associated with a decrease in microCT2.5 level. In contrast, increases in CTP prevalence among TS cells and in the BMA were associated with an increase in microCT-2.5 level.

BMA.cellularity	-7.7384	7.0756	-1.094	0.28709
BMA.CTP.Prevalence	22.0851	11.7784	1.875	0.07547 .
MS.cellularity	5.8056	5.1634	1.124	0.27416
MS.CTP.Prevalence	-11.0632	7.2596	-1.524	0.14318
TS.cellularity	4.4504	6.6696	0.667	0.51223
TS.CTP.Prevalence	2.7982	0.8675	3.225	0.00424 **
Graft_Histo_cartilage	-0.6553	21.4711	-0.031	0.97596
Graft_Histo_.bone	45.5486	46.6194	0.977	0.34022
Graft_Histo_hematopoetic.marrow	-14.7145	25.1369	-0.585	0.56484
Graft_Histo_adipose.tissue	-3407.3018	1886.5932	-1.806	0.08598 .
Graft_Histo_vasculature.area	-254.3541	3743.0822	-0.068	0.94650

Table 11 - Linear regression metrics for microCT-2.5 model for group 5.

4. Effects of spacer texture and membrane scraping on microCT-2.5 level and X-ray healing rank

We also investigated if spacer texture and membrane scraping could predict microCT-2.5 level and X-ray healing rank. The response variables membrane scraping and spacer texture are both binary outputs so we ran logistic regression models. Membrane scraping did not significantly affect microCT-2.5 levels and X-ray healing rank as shown in table 12. Spacer texture did not significantly affect microCT-2.5 levels and X-ray healing rank as shown in table 13.

	Estimate	Std. Error	z value	Pr(> z)
(Intercept)	-0.9585444	2.7714776	-0.346	0.729
CT.2.5	0.0009173	0.0023906	0.384	0.701
CT.5	-0.0001429	0.0011803	-0.121	0.904
Xray.Rank	0.0198139	0.1119994	0.177	0.860

Table 1 - Logistic regression statistics for membrane scraping

Coefficients:				
##	Estimate	Std. Error	z value	Pr(> z)
## (Intercept)	4.281593	2.941563	1.456	0.146
## CT.2.5	0.002070	0.002326	0.890	0.374
## CT.5	-0.001507	0.001269	-1.188	0.235
## Xray.Rank	-0.154293	0.113735	-1.357	0.175

Table 13 - Logistic regression statistics for spacer texture

5. Effect of spacer texture on IM biology.

We model the response of spacer texture on IM biology as shown below using a logistic regression equation. We found that IM vascularity was significantly affected by spacer texture.

Coefficients:

##	Estimate	Std. Error	z value	Pr(> z)
## (Intercept)	3.415e+01	1.582e+04	0.002	0.9983
## Tib_Histo_Bone.Area..3.5	3.854e-03	4.161e-03	0.926	0.3543
## IM_Histo_Vascularity	5.932e+00	3.110e+00	1.907	0.0565
## IM_Histo_Fibrosis	-1.020e+01	3.956e+03	-0.003	0.9979
## IM_Histo_inflammatory_Cellularity	-8.033e-02	3.932e+00	-0.020	0.9837
## IM_Histo_Thickness	-1.631e+00	1.021e+00	-1.598	0.1101
## IM.membrane._.weight	2.428e+01	1.991e+01	1.220	0.2226
## IM_Inner.Mean.cellularity	-5.237e-02	7.743e-02	-0.676	0.4988
## Day6.IM_inner.cells	2.545e-04	2.339e-04	1.088	0.2766
## IM_Outer.Mean.cellularity	7.689e-02	3.044e-01	0.253	0.8006
## Day6.IM_outer.cells	3.979e-04	5.917e-04	0.673	0.5013

Table 14 - Logistic regression metrics for spacer texture and IM biology predictors.

6. Effect of spacer texture on gene expression

Our modeling of genes expression due in relation to spacer texture using the logistics regression equation did not succeed. The scale of the data collected rendered the algorithm unapplicable. We resorted to applying various analytics techniques to overcome the poor data quality. Important genes selection was performed by running random forest, **Boruta**, **Lasso**, **pda**, and **nnet**. Figure 19 shows in green the most important genes that were influenced by the spacer texture in the inner section.

The more stringent variable selection algorithm is shown to be Lasso (Glmnet) that selected only TGFB1, ALPL, PDGFB, OCT4, and IBSP as important genes expressed in the inner IM section (Table 14) affected by the spacer texture. The genes consistently ranked on the top of the list was used to build and predictive models of gene expression in the inner section. Table 14 shows in descending order the list of importance genes as sorted by the Random forest analysis and Table 15 shows in descending order the list of importance genes as sorted by neural network.

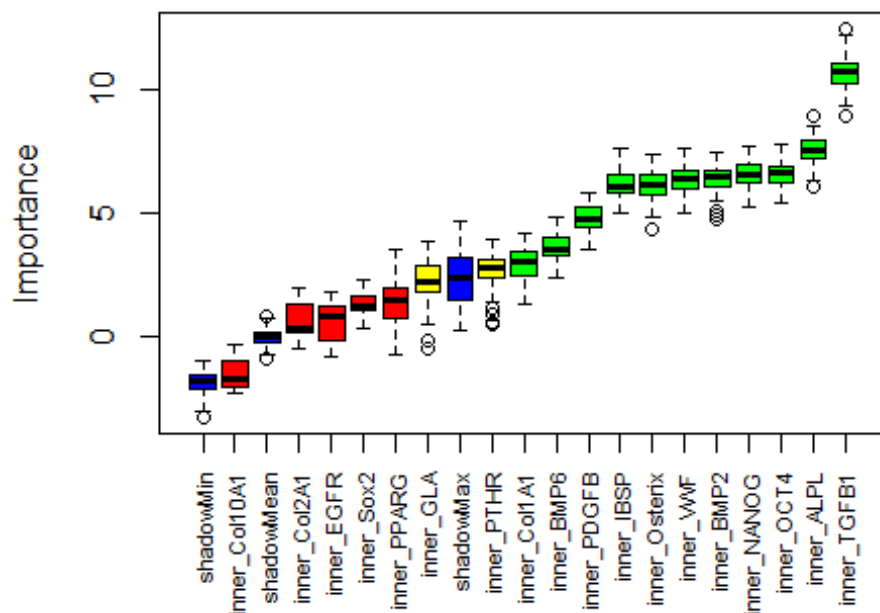


Figure 19 – Important genes in the inner section in response to spacer texture.

```

glmnet variable importance
##
##
## Overall
## inner_TGFB1 100.000
## inner_ALPL 27.017
## inner_PDGFB 19.374
## inner_OCT4 14.761
## inner_IBSP 2.777
## inner_PTHR 0.000
## inner_VWF 0.000
## inner_Sox2 0.000
## inner_BMP2 0.000
## inner_PPARG 0.000
## inner_Col2A1 0.000
## inner_NANOG 0.000
## inner_Osterix 0.000
## inner_Col10A1 0.000
## inner_BMP6 0.000
## inner_EGFR 0.000
## inner_GLA 0.000
## inner_Col1A1 0.000

```

Table 15 - Important genes found ranked by Lasso (Glmnet)

```

## rf variable importance
##
## Overall
## inner_TGFB1 100.000
## inner_OCT4 67.666
## inner_PDGFB 66.852
## inner_ALPL 63.674
## inner_IBSP 61.751
## inner_NANOG 61.396
## inner_VWF 60.564
## inner_Osterix 59.188
## inner_BMP2 53.059
## inner_Col1A1 30.023
## inner_BMP6 29.087
## inner_PTHR 24.297
## inner_GLA 21.041
## inner_Col2A1 14.807
## inner_Col10A1 9.303
## inner_EGFR 8.370
## inner_PPARG 3.780
## inner_Sox2 0.000

```

Table 16 - Important genes found ranked by Random Forest analysis

```

nnet variable importance
##
##
## Overall
## inner_TGFB1 100.000
## inner_ALPL 70.821
## inner_OCT4 61.220
## inner_PDGFβ 50.580
## inner_VWF 48.515
## inner_Col10A1 47.822
## inner_BMP2 37.931
## inner_Osterix 29.759
## inner_Col2A1 20.475
## inner_PPARG 19.714
## inner_EGFR 18.727
## inner_BMP6 17.232
## inner_PTHR 16.065
## inner_IBSP 15.546
## inner_NANOG 11.725
## inner_Sox2 10.468
## inner_Col1A1 6.657
## inner_GLA 0.000

```

Table 17 - Important genes found ranked by neural network

The same analytic approach to model design was applied to genes in the outer IM sections. Boruta displays in Figure 20 the important genes expressed in the outer section. Tables 18, 19, and 20 show the lists of important genes that were significant predictors of spacer texture. The more stringent variable selection algorithm is shown to be Lasso (Glmnet) which selected only BMP6, TGFB1, BMP2, ALPL, PTHR, Col1A1, Sox2 as important genes expressed in the outer IM section affected by the spacer texture (Table 18).

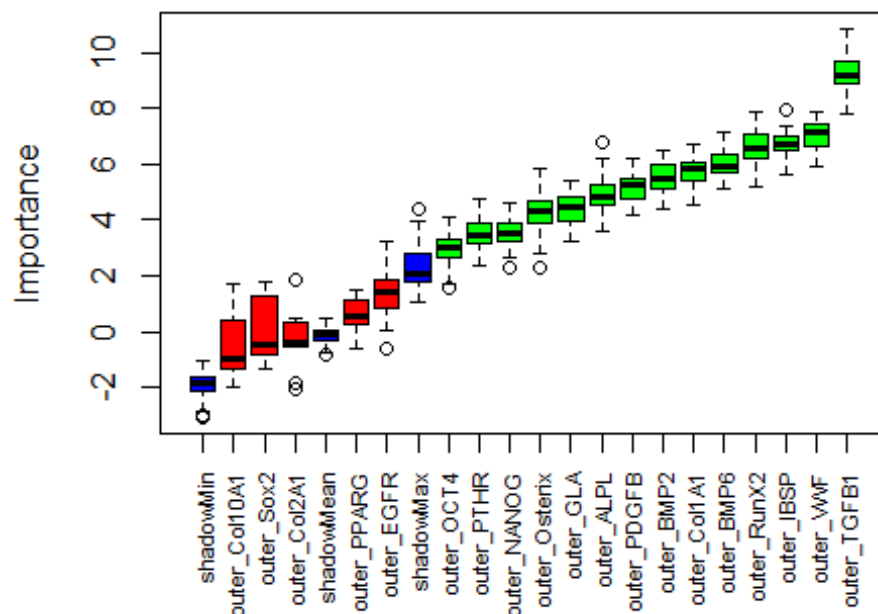


Figure 20 – Importance of genes in the outer section in response to spacer texture.

```
## glmnet variable importance
##
## Overall
## outer_BMP6      100.00
## outer_TGFB1     65.76
## outer_BMP2      54.40
## outer_ALPL      28.92
## outer_PTHR      25.93
## outer_Col1A1    20.30
## outer_Sox2      14.43
## outer_Col10A1    0.00
## outer_PDGFB     0.00
## outer_GLA       0.00
## outer_VWF       0.00
## outer_OCT4      0.00
## outer_Osterix   0.00
## outer_IBSP      0.00
## outer_EGFR      0.00
## outer_PPARG     0.00
## outer_NANOG     0.00
## outer_RunX2     0.00
## outer_Col2A1    0.00
```

Table 2 - Important genes in the outer section in response to spacer texture found ranked by Glmnet (Lasso)

```
## Overall
## outer_TGFB1     100.000
## outer_IBSP      82.716
## outer_VWF       80.320
## outer_RunX2     73.534
## outer_GLA       65.553
## outer_BMP2      62.537
## outer_ALPL      61.800
## outer_BMP6      54.579
## outer_PDGFB     52.261
## outer_Osterix   51.092
## outer_Col1A1    48.436
## outer_PTHR      45.921
## outer_OCT4      35.961
## outer_NANOG     33.978
## outer_EGFR      17.501
## outer_Col2A1    7.987
## outer_PPARG     5.826
## outer_Sox2      4.712
## outer_Col10A1   0.000
```

Table 3 - Important genes in the outer section in response to spacer texture found ranked by Random Forest

```
## nnet variable importance
##
## Overall
## outer_TGFB1 100.000
## outer_OCT4 68.553
## outer_PPARG 67.519
## outer_BMP6 62.924
## outer_BMP2 56.754
## outer_RunX2 49.284
## outer_IBSP 39.539
## outer_Osterix 36.456
## outer_Sox2 33.667
## outer_PTHR 24.830
## outer_Col2A1 20.113
## outer_PDGFB 14.433
## outer_VWF 14.328
## outer_ALPL 13.649
## outer_Col1A1 11.827
## outer_EGFR 9.839
## outer_NANOG 7.592
## outer_GLA 5.417
## outer_Col10A1 0.000
```

Table 20 - Important genes in the outer section in response to spacer texture found ranked by neural network

3.3 Nested development award (NMRC/WRNMC - Dr. D'Alleyrand)

Dr. D'Alleyrand continued his interactions with Drs. Pluhar and Muschler and the veterinary staff at Cleveland Clinic during the animal surgeries in Aim 2. He became engaged and knowledgeable regarding the animal care process and participated in laboratory discussions. He had received more specialized training and orientation to microCT analysis, both on a theoretical and practical level. He worked with raw CT images and gained operating experience with the process of moving from raw images to quantitative data, including sources of variation and error. He participated in the process of preparing summary data, presentation materials and contributed as an author and editor for manuscript submissions and gave presentations in selective settings (e.g. OTA, SOMOS).

4. KEY RESEARCH ACCOMPLISHMENTS:

- All surgeries and all animal care in this project have been completed.
- All microCT data have been performed for Aim 1 and Aim 2 and showed significantly increased bone formation in the scraped membrane group, however there was no significant improvement of bone healing when textured versus smooth spacers were used.
- Histomorphometry data from the Aim 1 and Aim 2 tibia samples are consistent with the data obtained in the microCT analysis.
- The characterization of the cellularity and prevalence of osteogenic connective tissue progenitors from the induced membrane showed that individual induced membranes varied widely in weight, cellularity, and CTP prevalence. The inner layer of the membrane was more cellular than outer layer, but there were no differences in Day 6 cultured cell counts.
- We demonstrated that the IM is composed of two distinctive portions: a thin glistening inner surface, comprised of a cellular layer with some vessels, and an outer part of fibroblasts and collagen. Of

particular note, we demonstrated that the inner surface of the IM has higher levels of gene expression for PPARG and trends for lower expression of five other osteogenic genes (TGFB1, BMP2, BMP6, Col1A1 and PTHR). This may explain why surgically removing this layer benefits bone regeneration.

- We demonstrated the value of predictive modeling in the CCTD model and the power of this model for dissection of the complex relationships between biological variables and outcome.
 - We demonstrated that IM membrane biology was associated with differences in outcome. Increased expression of Col1A1 and BMP2 had a positive effect on CT2.5 ($p < 0.05$), while Sox2 BMP6, Col10A1 and GLA were trended toward significance. However, in increased expression of BMP6 and GLA were associated with decreased CT2.5.
 - We demonstrated that ACBG and BM quality were associated with significant differences in bone formation (CT2.5). Increases in CTP prevalence among TS cells and in the BM was associated with an increase in CT2.5. Increases in ACBG adipose tissue composition was associated with a decrease in CT2.5.
 - While spacer texture was not associated with a change in bone formation, it was associated with changes in gene expression within the IM, specifically TGFB1, ALPL, PDGFB, OCT4, and IBSP.

5. CONCLUSIONS:

Experience to date clearly shows that the CCTD model raises the biological bar for bone regeneration research and development. These data establish the CCTD model as the most rigorous and clinically relevant large animal model for testing new bone regeneration materials and therapies.

This study highlights that CCTD Model proved to be sensitive to detect variations in:

- Surgical technique (scraping)
- Spacer Design (biomaterial, texture, drug delivery)
- Graft quality (ACBG adipose and CTP prevalence and BM CTP prevalence)

Surgical removal of the inner surface of the IM significantly increased bone regeneration ($p = 0.041$), a finding that can be immediately translated into clinical practice.

Modifying the texture on the PMMA spacer to double the surface area of the IM did not result in improved bone regeneration. However, surface modification did change the gene expression within the resulting IM leaving open the opportunity to examine other spacer approaches.

The CCTD model is particularly well suited to advance the field of clinical bone regeneration using cellular therapies and optimization of clinically relevant methods for harvest and processing of CTP sources to enhance the concentration and prevalence CTPs in the site of bone regeneration. As these data demonstrate, ACBG and BM harvested from the caprine sternum is comparable to human clinical tissues in terms of content, concentration and prevalence of CTP. Moreover, the CCTD model is sensitive to changes in bone graft quality and the concentration and prevalence of CTPs.

The CCTD model is also well positioned to advance our understanding of the biological attributes of the IM and to explore means of optimizing these attributes through the use of spacers and other materials. Histological analysis of the induced membrane samples with a smooth PMMA spacer generates a relatively bland collagenous matrix of variable thickness with low cellularity and moderate vascularity, covered by a thin inner surface layer (foreign body response) with rare inflammatory cells, covering an underlying vascular plexus that varies in density. We also demonstrated that the IM is composed of two distinctive portions: a thin glistening inner surface, comprised of a cellular layer with some vessels and an outer part made of fibroblasts and collagen. Of particular note, we demonstrated that the inner surface of the IM has higher levels of gene expression for PPARG and tends to have a lower expression of five other osteogenic genes (TGFB1, BMP2, BMP6, Col1A1 and PTHR), which may explain why surgical removal of this layer benefits bone regeneration.

Our understanding of the cellular biology of the IM remains incomplete. Cell analysis of the induced membrane demonstrated that it contains substantial number of cells, including CTPs with osteogenic and chondrogenic potential. We were able to measure CTP prevalence in only four animals, however, due to the fact that CTP prevalence in the IM was greater than expected and plated samples were overrun with cells making colony formation impossible to discern. The fact that the IM may be a rich source of CTPs may have a positive or negative effect on bone regeneration depending on the biological potential and tendency for commitment of the cells that are present. Further assessment into the nature of the cell population that is resident in the IM and their independent contributions to bone regeneration presents opportunities for targeting and optimization of this cell source for bone regeneration using the CCTD model.

6. PUBLICATIONS, ABSTRACTS, AND PRESENTATIONS:

a. Publication:

1. This research was featured as a highlighted study in the Congressionally Directed Medical Research Programs FY16 Annual Report.
2. Luangphakdy V, Pluhar GE, Piuizzi NS, D'Alleyrand JC, Carlson C, Bechtold J, Forsberg J, Muschler GF. The Masquelet induced membrane technique: Optimizing surgical technique and spacer design. Submitted on Nov. 30th, 2016 to Clinical Orthopaedics and Related Research.

b. Presentations:

1. Weinzierl A, Toth F, Pluhar GE, Muschler GF, Bechtold J, Luangphakdy V, Carlson C, Histomorphometric Comparison of Graft Efficacy Using a Caprine Chronic Tibial Defect Model. ORS, 2015, Las Vegas, Nevada, March 28-31, 2015.
2. Luangphakdy V, Pluhar E, Zachos TA, Boehm C, Liu X, Carlson C, Bechtold JE, D'Alleyrand JC, Muschler GF, Optimizing Soft Tissue Management and Spacer Design in Segmental Bone Defects. ORS, Orlando, Florida, March 5-8, 2016.
3. Muschler GF, Luangphakdy V, D'Alleyrand JCD, Carlson C, Bechtold J, Pluhar GE, Optimizing soft tissue management and spacer design in caprine segmental bone defects, 2016 MHSRS, Orlando/Kissimmee, Florida, August 15-18, 2016.
4. Luangphakdy V, Boehm C, Zachos TA, D'Alleyrand JCD, Carlson C, Bechtold J, Pluhar GE, Muschler GF, Optimizing Soft Tissue Management And Spacer Design In Caprine Segmental Bone Defects. Podium presentation, 2016 TERMIS-AM Meeting, San Diego, California, December 11 – 14, 2016.
5. Muschler G, Luangphakdy V, Piuizzi N, D'Alleyrand JCD, Carlson C, Bechtold J, Pluhar GE, The Masquelet Induced Membrane Technique: Optimizing surgical technique and Spacer Design. Podium presentation, 69th Annual Meeting of The Association of Bone and Joint Surgeons in Austin, Texas, April 5-9, 2017.

7. INVENTIONS, PATENTS AND LICENSES:

Nothing to report

8. REPORTABLE OUTCOMES:

The Chronic Caprine Tibial Defect (CCTD) model raises the biological bar for clinically relevant preclinical assessment of advanced bone regeneration strategies. The CCTD model is now unequivocally the most rigorous, quantitative, and clinically relevant large animal model currently for testing new bone regeneration materials and therapies.

This study highlights that Chronic Caprine Tibial Defect Model is sensitive variations in surgical technique (scraping), spacer design (biomaterial, texture, drug delivery) and graft quality (ACBG adipose content and CTP prevalence and BM CTP prevalence)

Surgical removal of the inner surface of the IM significantly increased bone regeneration. This finding is important, clinically relevant and immediately translatable into clinical practice to serve wounded warriors as well as civilians.

9. OTHER ACHIEVEMENTS:

ASTM International has initiated a work group led by Dr. Pluhar (ASTM division IV TEMP, F04.44.) to develop the CCTD model as an ASTM Standard Method, recognizing the value of the CCTD model to the bone regeneration community.

10. REFERENCES:

1. Johnson, E.N., et al., Infectious complications of open type III tibial fractures among combat casualties. *Clin Infect Dis*, 2007. **45**(4):409-15.
2. Viateau, V., et al., Induction of a barrier membrane to facilitate reconstruction of massive segmental diaphyseal bone defects: an ovine model. *Vet Surg*, 2006. **35**(5): p. 445-52.
3. Masquelet, A.C., et al., [Reconstruction of the long bones by the induced membrane and spongy autograft]. *Ann Chir Plast Esthet*, 2000. **45**(3): p. 346-53.
4. Masquelet, A.C. and T. Begue, The concept of induced membrane for reconstruction of long bone defects. *Orthop Clin North Am*, 2010. **41**(1): p. 27-37; table of contents.
5. Giannoudis, P.V., et al., Masquelet technique for the treatment of bone defects: tips-tricks and future directions. *Injury*, 2011. **42**(6): p. 591-8.
6. Karger, C., et al., Treatment of posttraumatic bone defects by the induced membrane technique. *Orthop Traumatol Surg Res*, 2012. **98**(1): p. 97-102.
7. Standard Test Method for Automated Colony Forming Unit (CFU) Assays – Image Acquisition and Analysis Method for Enumerating and Characterizing Cells and Colonies in Culture, A. International, Editor. 2012.
8. Stekhoven, D.J. and Buehlmann, P. (2012), 'MissForest - nonparametric missing value imputation for mixed-type data', *Bioinformatics*, 28(1) 2012, 112-118.
9. Miron B. Kursu, Witold R. Rudnicki (2010). Feature Selection with the Boruta Package. *Journal of Statistical Software*, 36(11), p. 1-13.
10. Tibshirani, R. (1996) Regression shrinkage and selection via the lasso. *J. Royal. Statistics. Soc. B.*, Vol. 58, No. 1, 267-288.
11. Venables, W. N. \$Ripley, B.D. (2002) *Modern Applied Statistics with S*. Fourth edition. Springer, New York.
12. Breiman, L. (2001), *Random Forests*, *Machine Learning* 45(1), 5-32.

11. **APPENDICES:** Attach all appendices that contain information that supplements, clarifies or supports the text. Examples include original copies of journal articles, reprints of manuscripts and abstracts, a curriculum vitae, patent applications, study questionnaires, and surveys, etc.

Appendix # 1: Manuscript “The Masquelet induced membrane technique: Optimizing surgical technique and spacer design” Submitted on Nov. 30th, 2016 to Clinical Orthopaedics and Related Research.

The Masquelet induced membrane technique: Optimizing surgical technique and spacer design

Viviane Luangphakdy, MS, G. Elizabeth Pluhar, DVM, PhD, Nicolás S. Piuizzi, MD, Jean-Claude D'Alleyrand, MD, Cathy S. Carlson, DVM, PhD, Joan E. Bechtold, PhD, Jonathan Forsberg, MD, PhD, George F. Muschler, MD

Abstract

Background: The Masquelet induced membrane technique is a commonly used method for treating segmental bone defects. However, there are no established clinical standards for management of the spacer-induced membrane (IM) prior to grafting.

Questions/purposes: Two clinically-based hypotheses were tested in the Caprine Chronic Tibial Defect model: 1) A textured spacer will increase IM surface area will increase bone regeneration; 2) Surgical scraping to remove a thin layer of the inner IM surface will enhance bone formation.

Methods: Thirty-two female goats were assigned to four groups: smooth spacer with/without membrane scraping and textured spacer with/without membrane scraping. An initial surgery created a composite defect by excising 5cm of bone, 9cm of periosteum and 10g of muscle. Segments were stabilized with an intramedullary rod and an antibiotic-impregnated polymethylmethacrylate spacer with smooth or textured surface was implanted. Four weeks later, the spacer was removed and the IM was either scraped or left intact before autogenous cancellous bone grafting. Bone formation was assessed using xrays, microCT and histology at 16 weeks.

Results: MicroCT analysis demonstrated significantly greater bone formation in defects with scraped IM compared to defects with intact IM ($p=0.041$). There were no significant differences in bone formation detected between textured and smooth spacers ($p=0.47$).

Conclusion: Scraping the IM surface provided a more vascular environment that promoted bone regeneration; however increasing the surface area had no effect.

Clinical Relevance: Scraping the IM during the second stage of the Masquelet technique is a rapid and simple means of improving healing of segmental defects.

Introduction

Segmental bone defects represent a major, unsolved clinical challenge in orthopaedic practice, both in civil and military populations.[4, 5, 20, 23, 25] A critical segmental defect, defined as an osseous defect in a particular bone that will not heal spontaneously during its lifetime, may be primary bone defects resulting from high-energy trauma, infection, or developmental deformities, or secondary bone defects that occur from fracture non-union, tumor resection, or revision surgery.[4, 9, 14, 26] In short, a critical segmental defect is a bone void that will not fill without intervention.[19] Although acute bone shortening may be performed for small defects between 1-3 cm, autogenous cancellous bone graft (ACBG) remains the standard of care for bone defects less than 5 cm in size.[19, 25] For larger bone defects, ACBG results in a high failure rate due to graft resorption and lack of consolidation.[14, 19, 25] For these large bone defects, different techniques and approaches have been described including distraction osteogenesis (to treat 5-10 cm defects), vascularized bone transfer (to treat 10-20 cm defects), induced membrane (IM) technique, commonly called the Masquelet technique (to treat 5-24 cm defects), and amputation.[3, 4, 14, 19, 25]

Masquelet et al. developed a relatively novel technique to repair large bone defect in two surgical steps: In the *first step* [1], a radical debridement and soft-tissue repair (if necessary) is performed, and a polymethylmethacrylate (PMMA) cement spacer loaded with antibiotic is placed in the bone defect. In this first procedure the segmental defect may be stabilized by an intramedullary rod or by a plate. In the *second step* [2], performed four to eight weeks later, the PMMA spacer is removed and bone graft material is placed within the membrane envelope to fill the defect site. [15–18]

The present study addresses the treatment of segmental bone defects and technical methods to optimize the induced membrane technique using a caprine chronic tibial defect (CCTD) model. This protocol uses a Masquelet technique to create an induced membrane (IM) around a critical bone defect in a severely traumatized tissue bed. It involves creating a clinically relevant composite tissue defect in mature animals by excising 5 cm of tibia, 9 cm of periosteum, 10 gm of muscle, stabilization with a locking intramedullary rod and placement of an antibiotic-impregnated bone cement spacer four weeks prior to ACBG grafting. Two clinically based hypotheses were tested: **1)** The use of a textured spacer during the first stage of the Masquelet technique, that doubles the inner surface area of the IM will increase bone formation after grafting. **2)** Surgical scraping during the second stage of the procedure to remove a thin (1-2 mm) layer of the inner surface of IM will enhance bone formation after bone grafting.

Materials and Methods

Thirty-two skeletally mature female goats, age 5 ± 1 years (mean \pm SD) weighing 50 ± 4 kg underwent the CCTD procedure and were randomly assigned to four groups (8 animals/group) using a 2x2 test matrix (factorial design). These groups included: (1) smooth spacer and intact IM; (2) smooth spacer and scraped IM; (3) textured spacer and intact IM; and (4) textured spacer and scraped IM. Study animals were cared for in accordance with the principles of the Guide for the Care and Use of Laboratory Animals[22] after approval from the Cleveland Clinic Institutional Animal Care and Use Committee (IACUC # 2013-1021) and the Animal Care and Use Review Office of US Army Medical Research and Materiel Command (OR # 120082).

Caprine chronic tibial defect (CCTD) model

Prior to each surgery, goats were given perioperative analgesia using a fentanyl patch and a dual patch application approach. Medetomidine (0.025 mg/kg IM) and ketamine (0.5–1.0 mg/kg IM) were given for anesthetic induction to place an endotracheal tube and anesthesia was maintained with isoflurane 1.0–2.0% in oxygen. Cefazolin, 1 g IV, was given prophylactically just prior to and at the end of surgery. Morphine (0.1 mg/kg), diluted in 0.9% sterile saline to a volume of 0.13 ml/kg, was given for analgesia in the epidural space after induction.

During the first surgery, a “pre-procedure” established the critical bone defect. The surgery involved a medial approach to the left tibia and removal of a 5 cm mid-diaphyseal osteoperiosteal segment. Additional 2-cm segments of periosteum on either side of the defect and 10 gm (~ 10 cm³) of skeletal muscle and fascia surrounding the defect site were removed. After the establishment of the critical bone defect, the first stage of the Masquelet technique was done. The tibia was stabilized with an 8-mm diameter, 185-mm long intramedullary interlocking nail (Innovative Animal Products, Rochester, MN) and the defect was filled with a polymethylmethacrylate cement spacer impregnated with vancomycin (0.5 g) and tobramycin (0.5 g) (Simplex P polymer, Stryker, Mahwah, NJ). As indicated previously, 16 goats were assigned to the smooth spacer group (**Figure 1A**) and the remaining 16 goats were assigned the textured spacer group (**Figure 1D**) during this first procedure.

The second surgery (Second stage of the Masquelet technique) was performed four weeks later, to remove the PMMA spacer through a medial approach using a “bomb bay door” opening technique. Two IM treatments were followed before the defect was filled with 10-12 cm³ of ACBG harvested from the sternum: a) scraped IM: the inner layer of the IM was removed with a curette (n = 16 goats) and b) intact IM: no manipulation of the inner IM layer (n = 16 goats). (**Figure 1B, C, E & F**) The induced membrane and skin were separately closed with 3-0 polydioxanone and nylon, respectively.

Post-operative pain management was administered using transdermal fentanyl patches (100µg/hr x 5 days) and phenylbutazone (1 g P.O.) as needed. Animals were allowed to be freely mobile and fully weight bearing immediately on recovery from anesthesia. They were housed in individual pens with free access to food and

water. The goats were checked twice daily for mentation/ attitude, ability to ambulate, willingness to bear weight on the operated limb, food and water consumption, respiratory rate, and inflammation at the surgical site.

The goats were euthanized twelve weeks after the second surgery to harvest the entire left tibia, preserving the periosteum and fibrous tissue surrounding the defects. Samples were fixed in 10% neutral buffered formalin for 48 hours and then transferred to 70% ethanol (EtOH).

MicroCT processing and analysis

High resolution microCT was used as the primary outcome measure to characterize the amount and distribution of bone within each defect. Prior to scanning, the nail and screws were carefully removed and replaced with a radiolucent rod and cross-pins to maintain the original length and axial and rotational alignment. After centering in the scanner (Inveon microCT scanner, Siemens Medical Solutions, Knoxville, TN), 441 projection images were acquired at 0.5° increments at 39- μm voxel resolution (80 kVp; 500 μA). Data were reconstructed into 3D volumes using a modified tent-Feldkamp algorithm and calibrated to mg/cm^3 of HA using an air/water/hydroxyapatite phantom scanned under the same conditions. Bone threshold was set at 1300 mg/cm^3 (747 HU). The analyzed volume of interest (VOI) included the 5 cm defect region plus 1 cm of bone proximal and distal to the defect. Each specimen was analyzed with a segmentation software developed in-house, in which a 3-dimensional cylindrical “defect template” volume 45mm in diameter and 70 mm in length, was manually positioned to define the boundaries of the VOI. Primary outcome was defined as total bone volume (tBV) in the central 2.5 cm region of the defect, which is the most challenging region to heal.

Secondary outcomes were radial percent bone volume (%BV), a summation of circumferential bone volume over the length of the defect, and angle-moment of inertia in the defect site. Summary data of the pattern and extent of mineralization in the defects in each group were illustrated by projecting %BV versus radial position using a 2D color map ranging from 0% (purple) to 60% (red). The x-axis indicated distance from the center of the medullary canal to the periosteal surface (range = 0-29 mm). The y-axis represented the position in the long axis of the bone (range 0 - 70 mm) including the 5 cm defect plus 1 cm proximal and distal. Mean Angle-moment of inertia for each group was also plotted using a 2D color plot color map ranging 0 (purple) to 7000 Hounsfield units (HU)* mm^2 (red) plotted about the bone circumference in the x-axis and the long bone axis position in the y-axis.

Radiographic Analysis

Fluoroscopic imaging of the tibiae, anterior-posterior (AP) and medio-lateral (ML) projections, were performed after each surgery: Stage 1 (week 0), Stage 2 (week 4), and follow-up (week 8) (Figure 4). Radiographs were obtained after euthanasia (after soft tissues were dissected) and the images were ranked from 1 (greatest bone healing) to 20 (no healing) by two independent investigators (senior orthopaedic surgeon and junior orthopaedic surgeon) who were blinded to treatment allocation. The highest-ranking sites revealed bony bridging (bone extending the length of the defect with no discontinuity) of all four cortices, followed by bony bridging of three, two, one, or none of the cortices. Among samples that had the same number of bony bridges, the ranking was based on the subjective amount of bone observed.

Histology Analysis

Following microCT data collection, histology and histomorphometry were performed. Each fixed tibia was immersed in dilute HCl (~1 week) and then transferred to a 10% EDTA solution until completely decalcified. Decalcified specimens were embedded in paraffin, trimmed to 7 cm to include the 5 cm defect and 1 cm at either end. The specimens were compared with the corresponding faxitron radiographs to ensure that the correct tissue area was examined. The specimens were then divided into four 1.75 cm long segments that were then cut

in the craniocaudal direction on the mid-sagittal plane to yield medial and lateral halves. Medial halves (each including the anterior and posterior cortices) were processed in paraffin (four blocks/specimen), sectioned at 5- μ m, and stained with hematoxylin and eosin (H&E) and Masson's trichrome. For the histomorphometric analysis, total area of bone in the sections from the two central 1.75 cm blocks (total of 3.5 cm) was measured by tracing the perimeter of each individual focus/area of bone tissue in the section in both anterior and posterior cortices (mm^2) using SPOT basic histomorphometry software (SPOT Imaging, Sterling Heights, MI) and summing the results for each animal.

Statistical Analysis

A power analysis using previous data collected with this animal model was performed to estimate the sample size required for detecting a difference in new bone volume parameter. Using the traditional alpha set to 0.05, 16 goats (8 animals per group) provides a power of 0.78 to detect a change from 20% bone volume to 30%. This 10% difference, approximately 1 cm^3 , in this range of bone formation is considered to be clinically significant.

All statistical tests were performed using general linear models using one-sided tests at a significance level of 0.05 with SAS 9.4 software (SAS Institute, Cary, NC). The response variable was total bone volume (tBV in mm^3) calculated from the microCT scans in the central 2.5 cm of the defect and the treatment factors were scraped or non-scraped IM and textured or smooth spacers. All data were expressed as mean \pm standard error.

Results

Three goats were excluded due to complications. Two belonged to the intact/smooth group and were excluded due to Staphylococcus epidermidis infection (n=1) or caseous lymphadenitis (n=1); one goat in the scraped/smooth group was excluded due to anesthetic complication during stage 2 surgery (n=1).

Bone formation assessed by MicroCT

Mean radial tBV in the central 2.5 cm of the defect was significantly greater in the IM scraped group (mean \pm standard error = $1861.0 \pm 351.3 \text{ mm}^3$) vs. non-scraped IM ($930.3 \pm 390.3 \text{ mm}^3$) ($p = 0.041$). However, we were unable to demonstrate a significant difference between the smooth or textured spacer groups ($p = 0.475$) (**Figure 2**). The mean tBV in the central 2.5 cm of the defects was $1413.8 \pm 363.3 \text{ mm}^3$ for the smooth membrane group and $1377.5 \pm 377.5 \text{ mm}^3$ for the textured membrane group. These data are graphically presented using a heat map in Figure 3. Mean percent bone volume in Figure 3 illustrates that there is greater bone formation (>60%) near the osteotomy sites. The angle-moment of inertia plots illustrate that bone tended to form along the posterior and medial aspect of the defect with little bone formation laterally in the IM scraped group while in the intact IM group, new bone formation was found both medially and laterally. Textured and smooth spacer groups had comparable new bone formation, with bone preferentially forming posteriorly in both groups as shown in the angle moment plots.

Postmortem radiograph ranking

Overall, the scraped IM group ranked better than the non-scraped IM group based on previously described radiographic criteria (**Supplemental Figure 1**). Eight of the top ten top-ranked goats belonged to the scraped IM group. The radiographic ranking did not reveal any differences between smooth and textured spacer groups.

Histology

Histological assessment of the goat tibia samples identified no evidence of inflammation in any of the sections 12 weeks after grafting. The majority of the bone that was present in the sections was composed of cancellous

woven bone. There was a large amount of variation in the amount of bone present in the defects, with some defects completely filled with bone and others contained almost no bone. Defects containing little or no bone were filled primarily with fibrous connective tissue. The most robust bone regeneration occurred in the scraped IM group (mean total bone area = $244.1 \pm 67.8 \text{ mm}^2$) compared to the intact IM group ($177.0 \pm 74.3 \text{ mm}^2$), which is consistent with the microCT data. The histomorphometry data also showed that textured spacer group (mean total bone area = $296.9 \pm 94.3 \text{ mm}^2$) had a larger area of bone in the defect than smooth spacer group ($136.7 \pm 30.4 \text{ mm}^2$) but this difference was not statistically significant due to the large variation in the textured spacer group.

Discussion

The Masquelet technique is a novel and effective two-stage method to enhance bone reconstruction by creating a vascularized soft tissue envelope prior to grafting of bone defects.[2, 4, 6, 11, 15, 16, 18, 25, 28] Optimizing the Masquelet IM method and characterization of the biological features of the IM may have significant potential to enhance the clinical care of patients who require bone regeneration procedures to treat critical segmental bone defects. The main finding of this study was that the effect of scraping the inner surface of the IM during the second stage of the Masquelet technique was associated with improved bone formation and we were unable to find differences in the bone formation between different spacer designs.

The IM is composed of two portions: a thin glistening inner surface, synovial-like epithelium, comprised of protein exudate and minimal evidence of a foreign body reaction, and an outer part made of fibroblasts, myofibroblasts, and collagen.[24] It has been described previously as an organized richly vascularized pseudo-synovial membrane, that promotes the revascularization of the graft that is contained within the membrane and prevents its resorption.[13, 16, 24, 29] Many biological properties have been attributed to the IM, including expression of bone morphogenetic protein-2 (BMP-2), transforming growth factor- β , vascular endothelial growth factor (VEGF), von Willebrand factor, interleukin 6, interleukin 8, type 1 collagen, and stroma-derived factor 1, and it also has been described as a source of stem/progenitor cells.[1, 7, 8, 12, 24, 29, 30] Aho et al. showed that the IM osteogenetic capability with highest biological activity (VEGF expression and vascularity) was achieved one month after spacer implantation.[1]

Although the Masquelet technique is used worldwide[10] and a significant amount of basic and clinical research has been done on the IM technique, there are no established surgical standards to manage the IM inner surface prior to bone grafting. Removal of the glistening inner layer of the IM induces bleeding from a healthy vascular bed, while preserving the mechanical function of the rest of the fibrous envelope of the IM. This technical modification may represent a rapid and simple means of enhancing the biological environment of the tissue bed. Further investigations into the nature of the IM including those exploring resident cell populations and mechanism responsible for this effect, and additional means of optimizing the IM prior to bone grafting require further experimentation now in progress.

A textured spacer has been shown to be associated with more developed membrane synovial-like metaplasia and villous hyperplasia,[16] but the effect of spacer texture on bone healing is not well known. We tested a ribbed spacer, to double the IM surface area to try to enhance bone healing, however we were unable to demonstrate a significant difference in bone volume between the two spacer designs. We recognize thought that the study may have been underpowered to show a difference. There are several variables in the optimization of the Masquelet Technique that still require further research as: stabilization choice, type and amount of grafting material, optimal time allotted to each stage, the use of growth factors, and supplementation with cell-therapy.[4, 16, 20, 27, 29]

Advancement in surgical clinical care of critical bone defects is limited mainly by two key factors: 1) prospective clinical trials are expensive and time consuming; 2) available large animal models, generally present acute bone defects in young healthy animals, that heal reliably with many existing therapies, creating a

“ceiling effect”.[21] The CCTD model developed in our laboratory addresses the latter limitation and provides a robust model that hastens clinical translation. This study described here is among the first studies to employ randomization and a control group in a large animal model of bone healing to allow a head-to-head comparison in a model relevant to human care. While the CCTD model starts with a healthy biology and does not include complications like infection and debridement, it represents a demanding and exigent model for bone formation. Furthermore, new bone formation between treatments was assessed in the center-most 2.5 cm of the defect that is considered to be the most discriminating region with respect to healing efficacy in large defects, and therefore serving as the primary outcome parameter while histology is used as a secondary outcome to evaluate the quality of the new bone tissue formed (**Supplemental Figure 2**). Moreover this model was able to show a clear and significant difference in healing rates using different surgical manipulations of the Masquelet IM technique. Scraping the inner layer of membrane produced statistically improved bone growth. Notably, the mean cross-sectional area of bone produced was nearly doubled. These compelling results support the introduction of this modified Masquelet technique in complex surgical reconstruction in prospective studies.

Conclusion

The effect of scraping the inner surface of the IM during the second stage of the Masquelet technique is associated with improved bone regeneration. Scraping of the inner surface of the induced membrane increases bleeding from a healthy granulation tissue bed that enhances the biological environment while preserving the mechanical function of the IM as a fibrous envelope.

This study highlights the opportunity of optimizing surgical techniques to improve healing of segmental bone defects. The findings from this study can immediately be translated to the clinical care of civilians and military personnel.

Source of Funding

This work was funded by the Congressionally Directed Medical Research Programs Peer Reviewed Orthopaedic Research Program grant Award # W81XWH-13-2-0086.

Acknowledgments

We gratefully acknowledge Cynthia Boehm, Wesley Bova, Terry Zachos for their technical assistance during surgery; Dr. Kimerly Powell and Dr. Justin Jeffery for help with microCT processing and analysis; Ferenc Toth, Elizabeth Marchant and Channing Bancroft for help with histology processing and analysis; Xiaobo Liu for assistance with statistical analysis.

References

1. Aho O, Lehenkari P, Ristiniemi J, Lehtonen S, Risteli J, Leskela H-V. The Mechanism of Action of Induced Membranes in Bone Repair. *J. Bone Jt. Surg.* 2013;95–A:597–604.
2. Aparad T, Bigorre N, Cronier P, Duteille F, Bizot P, Massin P. Two-stage reconstruction of post-traumatic segmental tibia bone loss with nailing. *Orthop. Traumatol. Surg. Res.* 2010;96:549–553.
3. Ashman O, Phillips AM. Treatment of non-unions with bone defects: Which option and why? *Injury.* 2013;44:S43–S45.
4. Aurégan JC, Bégué T. Induced membrane for treatment of critical sized bone defect: A review of experimental and clinical experiences. *Int. Orthop.* 2014;38:1971–1978.
5. Brown K V., Guthrie HC, Ramasamy A, Kendrew JM, Clasper J. Modern military surgery: Lessons from Iraq and Afghanistan. *Bone Joint J.* 2012;94–B:536–543.
6. Chong K-W, Yi-Loong Woon C, Wong M. Induced Membranes—A Staged Technique of Bone-Grafting for Segmental Bone Loss Surgical Surgical Technique. *J. Bone Jt. Surg.* 2011;93:85–91.

7. Christou C, Oliver RA, Yu Y, Walsh WR. The Masquelet Technique for Membrane Induction and the Healing of Ovine Critical Sized Segmental Defects. *PLoS One*. 2014;1–19.
8. Cuthbert RJ, Churchman SM, Tan HB, McGonagle D, Jones E, Giannoudis P V. Induced periosteum a complex cellular scaffold for the treatment of large bone defects. *Bone*. 2013;57:484–492.
9. Domic-Cule I, Pecina M, Jelic M, Jankolija M, Popek I, Grgurevic L, Vukicevic S. Biological aspects of segmental bone defects management. *Int. Orthop*. 2015;39:1005–1011.
10. Giannoudis P V. Has the Induced Membrane Technique Revolutionized the Treatment of Bone Defects ? *Tech. Orthop*. 2016;31:2016.
11. Giannoudis P V, Faour O, Goff T, Kanakaris N, Dimitriou R. Masquelet technique for the treatment of bone defects: tips-tricks and future directions. *Injury*. 2011;42:591–598.
12. Gouron R, Petit L, Boudot C, Six I, Brazier M, Kamel S, Mentaverri R. Osteoclasts and their precursors are present in the induced-membrane during bone reconstruction using the Masquelet technique. *J. Tissue Eng. Regen. Med*. 2016.
13. Klaue K, Knothe U, Anton C, Pfluger H, Stoddart M, Masquelet AC, Perren SM. Research News from AO Bone regeneration in long-bone defects : tissue compartmentalisation ? In vivo study on bone defects in sheep. *Injury*. 2009;40S4:S95–S102.
14. Lasanianos NG, Kanakaris NK, Giannoudis P V. Current management of long bone large segmental defects. *Orthop. Trauma*. 2010;24:149–163.
15. Masquelet AC. The Evolution of the Induced Membrane Technique : Current Status and Future Directions. *Tech. Orthop*. 2016;31:3–8.
16. Masquelet AC, Begue T. The concept of induced membrane for reconstruction of long bone defects. *Orthop. Clin. North Am*. 2010;41:27–37; table of contents.
17. Masquelet AC, Fitoussi F, Begue T, Muller GP. [Reconstruction of the long bones by the induced membrane and spongy autograft]. *Ann. Chir. Plast. esthétique*. 2000;45:346–53.
18. Masquelet AC, Obert L. La technique de la membrane induite pour les pertes de substance osseuse de la main et du poignet. Induced membrane technique for bone defects in the hand and wrist. *Chir. Main*. 2010;29S:S221–S224.
19. Mauffrey C, Barlow BT, Smith W. Management of Segmental Bone Defects. *J Am Acad Orthop Surg*. 2015;23:143–153.
20. Mauffrey C, Hake ME, Chadayammuri V, Masquelet A-C. Reconstruction of Long Bone Infections Using the Induced Membrane Technique: Tips and Tricks. *J. Orthop. Trauma*. 2015;30:188–193.
21. Muschler GF, Raut VP, Patterson TE, Wenke JC, Hollinger JO. The design and use of animal models for translational research in bone tissue engineering and regenerative medicine. *Tissue Eng. Part B. Rev*. 2010;16:123–45.
22. National Research Council. Guide for the care and use of laboratory animals. 8th Editio. Washington, DC: National Academies Press; 2011.
23. Owens BD, Kragh JF, Macaitis J, Svoboda SJ, Wenke JC. Characterization of extremity wounds in Operation Iraqi Freedom and Operation Enduring Freedom. *J. Orthop. Trauma*. 2007;21:254–257.
24. Pelissier P, Masquelet AC, Bareille R, Mathoulin Pelissier S, Amedee J. Induced membranes secrete growth factors including vascular and osteoinductive factors and could stimulate bone regeneration. *J. Orthop. Res*. 2004;22:73–79.
25. Pipitone PS, Rehman S. Management of Traumatic Bone Loss in the Lower Extremity. *Orthop. Clin. North Am*. 2014;45:469–482.
26. Pneumaticos SG, Triantafyllopoulos GK, Basdra EK, Papavassiliou AG. Segmental bone defects: From cellular and molecular pathways to the development of novel biological treatments. *J. Cell. Mol. Med*. 2010;14:2561–2569.
27. Pountos I, Panteli M, Jones E, Giannoudis P V. How the Induced Membrane Contributes to Bone Repair : *Tech. Orthop*. 2016;31:9–13.
28. Ronga M, Ferraro S, Fagetti A, Cherubino M, Valdatta L, Cherubino P. Masquelet technique for the treatment of a severe acute tibial bone loss. *Injury*. 2014;45:S111–S115.

29. Viateau V, Bensidhoum M, Guillemin G, Petite H, Hannouche D, Fani A, Pelissier P. Use of the Induced Membrane Technique for Bone Tissue Engineering Purposes : Animal Studies. *Orthop Clin North Am.* 2010;41:49–56.
30. Viateau V, Guillemin G, Bousson V, Oudina K, Hannouche D, Sedel L, Logeart-Avramoglou D, Petite H. Long-Bone Critical-Size Defects Treated with Tissue-Engineered Grafts : A Study on Sheep. *J. Orthop. Res.* 2007;25:741–9.

Figure legends

Figure 1 – Surgery pictures showing placement of a smooth spacer (A) and textured spacer (D) in the defect site during the “pre-procedure” (Stage 1), the induced membrane four week later during the “treatment procedure” (Stage 2) after smooth spacer (B) or textured spacer (E) removal, and after scraping the smooth (C) and textured (F) IM.

Figure 2 – Total bone volume plots, based on microCT analyses, of the central 2.5 cm of the defect and the entire 5 cm defect illustrating the effect of scraping the IM (A) and the effect of the spacer texture (B).

Figure 3 – MicroCT plots illustrating the differences in bone formation and distribution. A) A radial color plot illustrates the probability of bone formation as the summation of the radial location relative to the vertical position in the defect. B) A Moment-Angle plot (bottom) illustrates that most bone formed on the posterior aspect of this defect. The proximal and distal borders of the defect are marked by dashed lines.

Figure 4 – Example of a series of tibial fluoroscopic images from a single goat taken during the experiment: A) after the “pre-procedure” surgery (Stage 1) showing the PMMA spacer in the defect site; B) after “treatment procedure” (Stage 2) 4 weeks later showing ACBG in the defect; C) at euthanasia (12 weeks after Stage 2 surgery) showing new bone formation in the defect site.

Figure 5 – Example of postmortem radiographs (AP and ML projections), MicroCT scan 3D reconstructions, % BV plot versus summation of radial position and Masson’s Trichrome stained histology slide for two goat tibias showing robust new bone (pink tissue) formation (A, B, C, D) or minimal new bone formation (E, F, G, H).

Supplementary figure 1 – Postmortem radiographs (AP and ML views) of the tibia from each goat used for ranking. Higher rank number indicates greater tibial bone formation (1 = complete bone healing to 29 = no healing).